A modular and stretchable electronic system for on-body health monitoring applications

by

Carlos Núñez López

Master of Science, Bioengineering
Swiss Federal Institute of Technology Lausanne, Switzerland (2017)

Licenciatura, Ingeniería Industrial
IQS School of Engineering, Spain (2014)

Submitted to the Program in Media Arts and Sciences, School of Architecture and Planning, in partial fulfillment of the requirements for the degree of

Master of Science in Media Technology

at the

Massachusetts Institute of Technology

September 2019

Author
. . . . . .

Program in Media Arts and Sciences
August 26, 2019

Certified by
. . . . . .

Joseph A. Paradiso
Professor of Media Arts and Sciences

Accepted by
. . . . . .

Tod Machover
Academic Head, Program in Media Arts in Sciences

A modular and stretchable electronic system for on-body health monitoring applications

by

Carlos Núñez López

Submitted to the Program in Media Arts and Sciences, School of Architecture and Planning on August 26, 2019, in partial fulfillment of the requirements for the degree of

Master of Science in Media Technology

Abstract

Most of current wearable devices used for health monitoring (e.g. Fitbit) are composed of bulky rigid electronics that are not customizable and are too rigid for the skin. To overcome such limitations, a modular system based on thin and stretchable electronic modules was proposed. To link modules together, a novel four pin sliding connector was designed, fabricated, integrated into an stretchable electronic circuit and characterized.

The first part of the thesis focused on investigating different stretchable conductive materials that could be integrated into soft rubber substrates. Two materials were tested. First, a commercial silver ink was deposited onto polyurethane rubber (PUR), showing high conductivity but minimum stretchability (below 3% strain). Second, serpentine shaped FPCs were designed and integrated into a silicone substrate, showing stretchability up to 160-170% strain with minimum changes in conductivity (below 30%). Additionally, a tensile cycling test showed stable electromechanical behavior up to 3,500 cycles at 30% maximum tensile strain.

The second part of this work addressed the design, fabrication and testing of a novel system for modular stretchable electronics. A four pin sliding connector to enable I2C communication was fabricated by assembling 3D printed parts with brass components manufactured with an EDM cutter. The mechanism could be easily integrated within the previously made stretchable FPC serpentines and demonstrated excellent electromechanical performance. A sample module could be stretched until complete serpentine failure (120% strain) with resistance values across the four pins lower than 2Ω. Furthermore, the device evaluation on a treadmill showed changes in resistance lower than 4.27Ω during the 15 minute experiments.

Thesis Advisor: Joseph A. Paradiso
Title: Professor of Media Arts and Sciences

A modular and stretchable electronic system for on-body health monitoring applications

by

Carlos Núñez López

This thesis has been reviewed and approved by the following committee members

Joseph A. Paradiso
. . . . . .

Professor of Media Arts and Sciences
Massachusetts Institute of Technology

Pattie Maes
. . . . . .

Professor of Media Arts and Sciences
Massachusetts Institute of Technology

Jue Deng
. . . . . .

Postdoctoral Fellow
Massachusetts Institute of Technology

Acknowledgments

I am immensely grateful to Prof. Joe Paradiso for being my advisor and caring so much about my work. He has been always available for me whenever I needed his guidance and we had numerous deep discussions about sensors, stretchable materials and career goals. Thank you so much for giving me the opportunity to be part of the Resenv family and for sharing your knowledge with me.

Second, I would like to thank my readers. Prof. Pattie Maes has been extremely supportive even before I joined Responsive Environments. She has shown a lot of enthusiasm about my work and given me prompt and detailed feedback. Dr. Jue Deng and my 'unofficial' reader Hyunwoo Yuk from the MIT Mechanical Engineering department were phenomenal. They offered me a lot of their time and expertise in stretchable electronics in our many meetings and e-mail exchanges.

I want to also thank my Resenv family: Brian, Mark, DD, Nan, Ariel, Juliana, David, Caroline, Ishwarya, Patrick, Elena, Fred, Yo, Clement, my UROP Ananya and my two favorite Italians: Manuel and Valentina. My special thanks to Artem (I should now call him Dr. Artem) for his contribution to this work in the sensor side of things.

This project wouldn't have been possible without the help of Will Langford and Tom Lutz from CBA. Thanks to them I could use this enormous machine called EDM (Electrical Discharge Machining) which was key to make the tiny brass connectors used in this work. Linda Peterson and Keira Horowitz, from the Media Lab academic program administration, were key to my survival during these two years and I am indebted to them.

Next, I would like to thank all my colleagues at the Media Lab who have been very supportive throughout these two years. Specially Tomás, Guillermo and Abhi from Fluid Interfaces who have given me many tips on sensors and PCB design as well as emotional support.

I am also very grateful to my first family I had when I arrived to MIT: Irmandy, Atieh, Zijun and Mohamed. Next, the Media Lab 'Spanish mafia': Pepe, Edu, Oscar and Marc. Outside the Media Lab I would like to thank my MIT Sloan family: Sophie, Jordi, Khat and Joseph. I also want to thank the constant emotional support of my besties, Khalil and Noaf, who have always been there by my side through my ups and downs.

Last but not least, I want to express my most sincere appreciation to my family. Especially to my parents Paqui and Luis as well as to my dear 'yaya' Pepita. They helped me to keep moving forward when I needed it most during these two years.

Contents

List of Figures

List of Abbreviations

Ag	Silver
CAD	Computer Aided Design
CNT	Carbon Nanotube
EDM	Electrical Discharge Machine
$EGaIn$	Eutectic Gallium-Indium
FPC	Flexible Printed Circuit
GPS	Global Positioning System
HR	Heart Rate
HCI	Human Computer Interaction
$I2C$	Inter-Integrated Circuit
MCU	Microcontroller Unit
NFC	Near-field Communication
$OTFT$	Organic Thin Film Transistor
PCB	Printed Circuit Board
$PDMS$	Poly-dimethylsiloxane
PI	Polyimide
PPG	Photoplethysmography
PU	Polyurethane
PUR	Polyurethane Rubber
RTV	Room Temperature Vulcanization silicone
SE	Standard Error
TPU	Thermoplastic Polyurethane

1 Problem statement

Most of high-performance electronics use inorganic materials, such as silicon or gallium arsenide, in a rigid and planar fashion [1]. On the other hand, the human body is made of soft and curvilinear surfaces, which limits the possibility of making devices that can conform to biological tissues. This is specially important when making wearable devices such as smart wristbands, where softness and comfort are key features to the user. Medical applications are another example, where patients may be using wearable technologies to monitor their vital signs or provide drugs for long periods of time. It is challenging to build integrated devices with sizes, weights and shapes that do not cause discomfort after continued use. [2].

The wearable device market is expected to grow up to $ 27 billion in 2022, which doubles the current sales in 2018 [3]. Smartwatches, specially those for health monitoring applications such as the Fitbit, are forecast to have the highest growth, well above other devices such as smart clothing, glasses and headphones. From their conception, smartwatches have attempted to replicate the shape and form factor of conventional watches. The first ever computerized wristwatch was created in 1972 by Pulsar, as it was capable of storing data [4]. However, the smartwatches as we know them today started in 2013 with devices like the Samsung Galaxy Gear [5], as the size and cost of hardware made it possible to integrate into the form factor of a watch a high number of sensors such as heart rate (HR) monitors, Global Positioning Systems (GPS) and pedometers.

Figure 1: Issues with current wearable smartbands. Image source: Garmin Forerunner 935 [6]

The main limitations of current wearable devices are represented in Figure 1 and summarized below:

- **Non-customizable components.** Most devices cannot be customized to have different hardware than the default when purchased. Users often dispose of gadgets to buy

new ones with additional features or upgrades. This is not only an economic burden for the user, but the e-waste also damages the environment.

- **Bulky electronic core.** All rigid electronic components are concentrated into a bulky electronic core on approximately one fourth of the device length (Figure 1). This makes wearables unevenly heavier and thicker along its perimeter, moving relative to the wrist (unless strapping devices too tight to the skin). This may cause accelerometers and gyroscopes to have signal artifacts (additional movement relative to the wrist) and HR sensors to fail detection (sensor detaches from the skin).

- **Poor adaptability to the skin**. Wearable straps are usually made of semi-rigid rubbers or leather to make them relatively comfortable to the user but strong enough to hold the rigid electronic core without breaking. Bovine leather is between two and three orders of magnitude stiffer than human skin (Young modulus of 94-100 MPa for cow leather [7] and 0.14-0.6 MPa for the epidermis [2]). Additionally, human limbs change in size subtly during the day, specially during physical activity due to fluid translocation across muscles that causes them to swell [8]. Variations in limb size are uncomfortable and causes users to constantly adjust the strap length.

- **No electronics on the strap.** Straps currently used in wearables are only designed to secure devices on our skin. However, sensors could benefit from better signal acquisition if they were placed in more strategic body areas. For example, doctors commonly use the palmar side of the wrist to take measurements of the pulse by touching the radial vein with their fingertips [9]. If smartwatches placed their HR monitors on the palmar side of the hand instead of the dorsal, signal acquisition could be greatly enhanced. Furthermore, distributing the electronics homogeneously throughout the device would distribute its size and weight along their perimeter.

2 Related work

This section covers the related work that sets the basis for this thesis, which aimed to make a soft and modular wearable system for on-body health monitoring applications. First, commercial wearable devices using flexible printed circuits (FPC) are introduced. Second, the most relevant modular wearables in the market are presented. Third, the emerging research field of stretchable electronics is reviewed as well as the fabrication strategies to integrate electronics into soft rubber. Last, recent research articles in modular stretchable electronic devices are discussed.

2.1 Wearables using flexible circuitry

A fitness tracker is a specific type of smartwatch that records a person's daily physical activity (e.g. amount of steps) and health data (e.g. heart rate) to monitor health or overall fitness. The popularity of these devices has boomed in the last ten years [10] and some companies have lead substantial design and engineering changes to solve some of the issues presented in Section 1.

Figure 2: Commercial smart wristbands using flexible PCBs. A) Jawbone UP and B) its exploded view [11]. C) Nike Fuel Band with the cover and D) without it [12]

A company named Jawbone produced in 2011 a smart wristband named "UP" which stood out from their competitors for achieving a slimmer design (See Figure 2A). Reduction in size was not only due to the non inclusion of a built-in screen, but the fact that electronics were distributed across the device perimeter. Discrete rigid PCB units such as the battery charger, flash memory and microprocessor were all interconnected by flexible circuitry to allow bending. Electronics were then fixed onto a sheet metal band to provide its curved

shape and encapsulated into a structural overmold with a hard button and a 3.5mm audio connector (See Figure 2B). Despite Jawbone efforts in making upgrades since their initial "UP" model and raising a valuation up to $3.4 billion in 2014, the company went out of business in 2017 [13]. Their flexible technology proved to be too expensive and prone to failure. The company claimed issues with two particular capacitors and users experienced difficulties to syncing with external devices [14].

Another company that used flexible circuitry for making fitness trackers was Nike with their model "FuelBand" in 2012 [12] (See Figure 2C). This smart band has all the electronics assembled in one long flexible circuit board with a low resolution screen for basic notifications. Hardware includes two batteries, a front button and a USB stick (See Figure 2D). Despite being bulkier than the Jawbone UP, this band gained momentum until Nike paused its production in 2016 to team up with Apple and make the Apple Watch Nike+ that same year [15].

Even though the market of fitness trackers is expected to decline with a reduction in sales of 10% in the next four years [3], a few companies have demonstrated clear innovation advancements to make wearables more flexible and modular.

2.2 Modular wearable devices

There are currently two commercial wearable smartbands that include modularity in their devices. BLOCKS is a smartwatch that began as a Kickstarter in 2015 and contains a main core with electronic segments that are snapped together with a multiple pin connector mechanism [16] (See Figure 3A). BLOCKS sells its main display module at a price of $259 and the other interchangeable modules at $35 each (HR monitor, environmental sensor, GPS, extra battery, etc).

Another example is the Nex Band, a smartband without display that has five notches to insert modules that add specific functions (eg. fitness tracking, messaging) or aesthetics [17] (See Figure 3B). However, this initial 2014 modular prototype has now evolved into a non-modular $38 commercial version where functions of five nodes can be customized (eg. smartphone shortcuts, notifications, fitness monitor, etc).

Figure 3: Modularity in commercial wearable devices. A) BLOCKS smartwatch, commercially available for $259 [16]. B) Nex Band, a modular smartband that has evolved into a non modular band in their first commercial release [17]. C) SensorTape, a modular flexible dense sensor network [18]

Modularity is also present in extremely thin configurations. Recently, researchers at the MIT Media Lab have fabricated a dense sensor network in a form factor of a tape that can be cut and rejoined to customize its shape [18] (Figure 3C). The electronic circuit is made using FPCs and modules are joined with one another using Z-tape, an adhesive tape that is electrically conductive on the Z-axis (perpendicular to the tape surface). Other research attempts to achieve modularity with small form factors can be found in Eco, a wireless device for infant monitoring and interactive dance that is under $1cm^3$ and can be expanded using flex-PCB connectors [19].

Another example of modularity but exclusively in terms of design is the Apple Watch. Different straps can be clipped to the electronic core using a thin profile mechanism as shown in Figure 4. The system is comprised of a female part on the sides of the watch core and a male part on the strap. The male part can be slided into the female sideways and it locks once both parts are aligned. The locking mechanism consists of a pin with a spring situated in the middle of the connector. Once the male part is aligned, the pin pops to keep both parts fixed. The user can release the strap by pressing the female pin, which in turn compresses the spring that allows free lateral movement of the male part. Even though most watches have the ability to interchange straps, this method stands out for being user friendly and not requiring any tools.

Figure 4: Apple watch and its modular design for customizing straps [20]

There are other companies outside of the wearable market that use modularity in their hardware. Littlebits is a Media Lab spinoff making an education oriented product that assembles LEGO-like electronic modules with magnets [21]. Another commercial example is Roli Blocks, a modular music synthesizer with magnetic connectors that allows users to assemble a custom made instrument [22]. Modular physiological sensing is commercialized by companies such as Libellum, BITalino, OpenBCI and OpenEEG, where electrodes and other sensors can be plugged into a controller board on demand.

2.3 Stretchable electronics fabrication techniques

The problem statement introduced how most of current electronics use materials that are rigid and planar while the human body is soft and curvilinear. Stretchable electronics is a growing field of research that aims to overcome such physical limitations to allow electronic materials to bend, twist and stretch. If electronics were made stretchable it could drastically impact a great number of medical applications, ranging from soft neural interfaces to medical monitoring to detect electrophysiological signals in cardiac tissue as well as skin moisture levels [23]. It could also introduce soft robotics to the market as well as changing how wearables are made [24].

One of the most common approaches to make flexible electronics is the placement of thin metallic and ceramic materials (hundreds of nanometers thick) on the device neutral axis to reduce strain (under 1%) [24], while the outer layers are made of softer materials accommodate the high compressive and tensile stresses [25]. The same approach is commercially used for making flexible printed circuits (FPC). However, these devices do not offer stretchability or ability to conform 3D curved surfaces.

One of the key aspects to fabricate electronic devices that comply to large deformations is the use of elastomeric substrates instead of rigid polymers as well as engineering the device geometry. Some of the most popular techniques are summarized in the following list and

introduced in Figure 5.

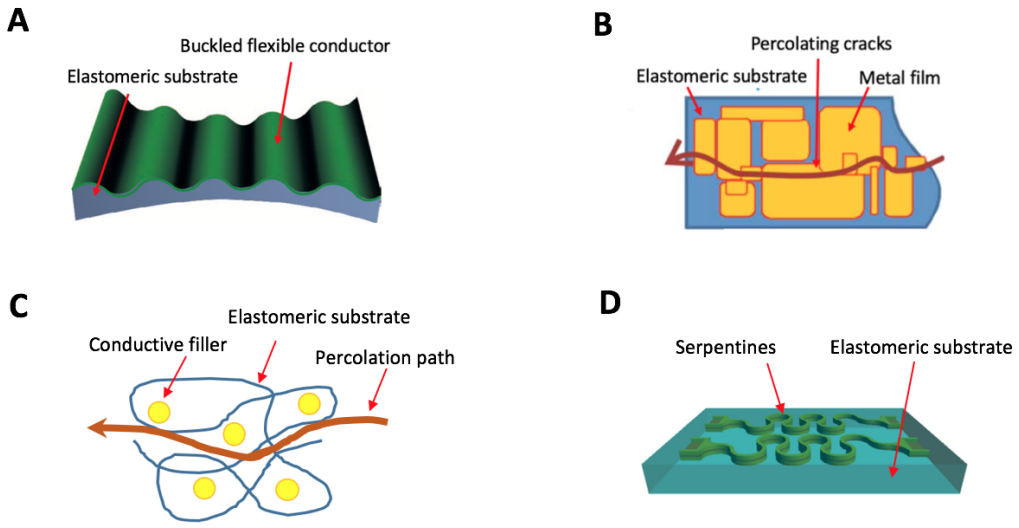

Figure 5: Main strategies to achieve stretchable conductors. A) Schematic of the buckling pre-stretching technique (adapted from [26]). B) Representation of the solid metal microcrack strategy (adapted from [25]) C) Schematic of the composite material technique. D) Representation of the serpentine structure strategy (adapted from [27])

- **Buckling.** This technology requires the attachment of a flexible device into a pre-stretched elastomeric substrate. Once the prestrained substrate is relaxed, the flexible device buckles out of the plane of deformation [28]. Furthermore, encapsulation layers can be added to the device to position the active components in the neutral plane and minimize strain. Main limitations of this approach are the change of sensing capabilities when bent and the restriction to applications than do not require full contact of the device with the target object [29]. See schematic in Figure 5A.

- **Solid metal microcracks**. Uses thermal evaporation of thin metallic layers onto thick elastomeric substrates. Devices can withstand high strains (up to 100%) with minimal changes in electrical resistance [30]. Tens of nanometer thick gold can be deposited on a stretchable substrate to form a network of gold ligaments spaced by microcracks, yielding conductivities just one order of magnitude lower than bulk gold [25]. This technology has allowed the development of soft neural interfaces for the spinal cord [31]. See schematic in Figure 5B.

- **Intrinsically stretchable materials**. Conductive stiff material particles or nanowires can be combined with insulating elastomers to make stretchable conductors [32]. Some examples of such technology are percolating networks of silver particles or carbon nanotubes (CNT) [33–35]. Other approaches involve the use of liquid metals such as mercury or gallium, which can be embedded in microfluidic channels or evaporated onto thin solid metals to make fine conductors [36, 37]. Figure 5C shows an schematic of the a conductive composite material. When the concentration of conductive filler

in an elastomer is high enough, resistivity falls exponentially due to the creation of a percolation path (See supplementary Figure 37). This approach has the advantage of being easy to process with screen-printing or ink-jet printing.

- **Serpentine structures**. Rigid conductive materials like gold or copper can be engineered to form serpentine/meander structures consisting of trilayer stacks of polymer/metal/ polymer. These constructs are two dimensional but can bend out of plane to accommodate strains [26]. Figure 5D shows a schematic of two coplanar serpentines embedded in an elastomer and Figure 6A displays serpentines bending out of plane. This strategy has been widely used in research [27, 38, 39] and external vendors manufacturing FPCs make it feasible to use this strategy both in research and industry.

Based on the techniques above, researchers have discovered ways to make complex stretchable electronic circuits that contain rigid components such as transistors, resistances and capacitors. One of the most popular methods is the "rigid island" approach, where rigid electronic components are distributed within an elastomeric substrate to evenly distribute stress concentrations. Rigid components are electrically connected using stretchable conductors such as out of plane deformation of serpentine-like structures (Figure 6A and B) or intrinsically stretchable silver composite materials (Figure 6C).

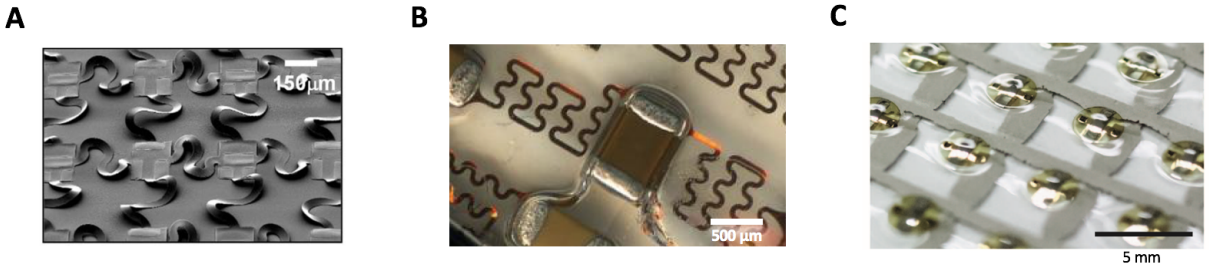

Figure 6: Rigid island strategy for making stretchable integrated circuits. A) SEM image of device islands that support transistors for CMOS inverters interconnected by conductive serpentines deforming out-of-plane [38]. B) Image of an stretchable system based on off-the-shelf resistors connected with serpentine interconnects and suspended in liquid to allow free out-of-plane buckling [39]. C) Organic thin film transistors (OTFT) interconnected with silver-rubber composite material [40]

Silver composites demonstrate several advantages over conductive serpentines for making stretchable electronics. Composites are easy to process, as they can be screen-printed using a polymer or metallic stencil. They are also commercially available from multiple vendors. DuPont, Engineered Materials Systems and Creative Materials manufacture composites based on thermoplastic polyurethane (TPU) and silver or carbon.

On the other hand, serpentine interconnects usually require multiple fabrication steps to achieve a polymer-metal-polymer trilayer and microfabrication is usually necessary to make thin features. Furthermore, rubber encapsulation of serpentines to increase device robustness reduces overall stretchability, as out of plane deformation is necessary to allow stretch.

To avoid this, there is research work that embeds serpentines in a liquid chamber to allow free buckling (Figure 6B).

Composite materials have several disadvantages compared to the serpentine strategy. First, conductivity is much lower than bulk metals like copper. Second, resistivity increases with the stress applied. Third, materials have relatively low resistance to fatigue due to the Mullins effect (separation of the filler particles from the polymer matrix) [41].

Researchers have also explored using liquid metals such as gallium or its alloys (eg. Gallinstan or EGaIn) as they can be strained up to high deformations with minimum changes in resistance. Such materials can be deposited using screen printing techniques [42] or microcontact printers [43, 44]. However, it is challenging to print traces that are thinner or pitched less than 0.5mm without short circuiting [42].

Besides the challenges mentioned above, making flexible electronics using gallium presents two other issues. Firstly, Gallium is highly reactive with other metals (eg. Cu, Al, Fe or Au), forming alloys, which can lead to the destruction of the contact between gallium and the embedded electronic components. Secondly, the oxide layer of Gallium is resistive, which can pose an issue for sensitive external electrical contacts [36].

2.4 Modularity in stretchable electronics

Modularity in stretchable electronics is a topic that has been largely unexplored until this year 2019. Three papers from different research institutes propose modular devices using stretchable electronics in unique ways.

First, researchers from Stanford University have developed modular electronics through self-healing materials that communicate with a standard I2C communication protocol (Figure 7A) [45]. Their technology is based on liquid gallium films deposited on a self-healing elastomer that can be cut and rejoined multiple times (Figure 7B). However, this type of chemistry is at its infancy and researchers claim material properties are still not comparable to non-healable functional electronic devices [46]. Indeed, Figure 7C shows the electromechanical performance of the device with a 5 to 50 fold increase in resistance when cut and rejoined multiple times and 500% differences in relative resistance when stretched to double its original length.

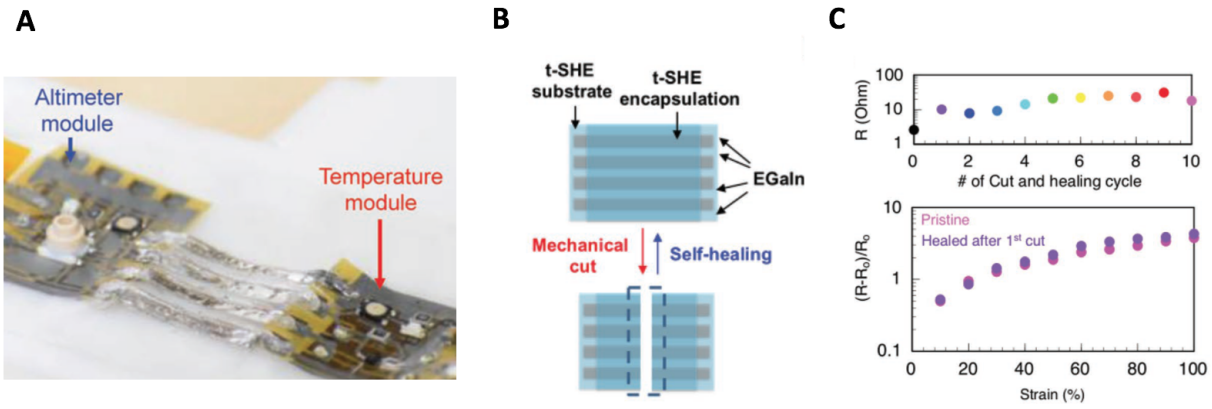

Figure 7: Stretchable and self-healable modular device. A) Two sensor modules with four lines for I2C communication. B) Self healing technology based on tough self healing elastomer (t-SHE) and liquid EGaIn. C) Resistance values when the self-healing material is cut and rejoined up to 10 times (top image) and relative changes in resistance after cut and rejoing the material (bottom image). Images reproduced with permission of Kang et al [45]

Second, researchers from University of Texas at Austin have made thin film stretchable e-tattoos that can be connected and disconnected multiple times by stacking one on top of each other (Figure 8) [47]. The system is made of a multilayer stack of three independent modules (NFC communication, ECG circuit and electrode module) which are interconnected through vias and double sided z-axis tape (Figure 8A). This strategy is similar to the one adopted by the SensorTape project (Figure 3D) [18] as they both use z-axis tape to connect exposed metallic pads between modules on top and bottom. The thin soft layer in contact with the skin is disposed after use due to the accumulation of skin dead cells but other layers can be reused for a minimum of 20 times. However, the extremely thin configuration of each elastomeric layer (Tegaderm, 47μm) does not make it practical or user friendly to manipulate the device layers as tweezers or other precision tools might be needed.

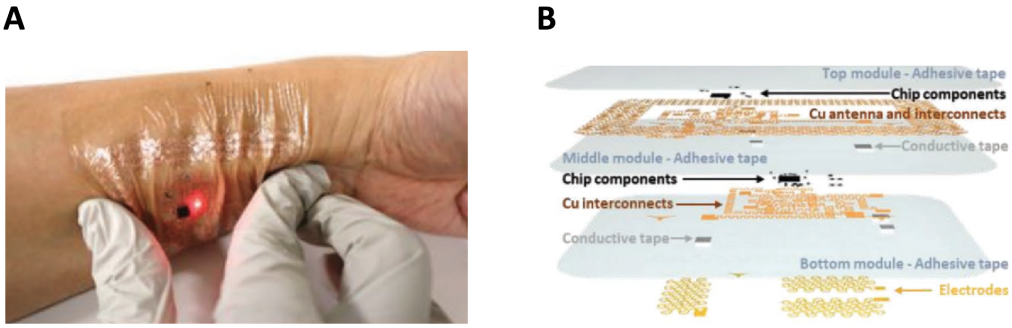

Figure 8: Stretchable modular e-tattoo. A) A wireless ECG device worn on the skin made of three layers: NFC, electronic circuit, and electrodes. B) Exploded view schematic of the three-layer wireless ECG device. Reproduced with permission of Jeong et al [47]

The third paper, published by researchers at Seoul National University, describes a system to interconnect stretchable electronic systems through conductive strips (Figure 9) [48]. Their technology consists of placing electronic blocks in any position on the skin and interconnecting them with a thin strip made of silver nanowire (AgNW) / PDMS silicone composite and the help of tweezers (Figure 9A). Stable electromechanical connection is ensured by surface-treating the conductive strips with oxygen plasma prior to the assembly. Despite the possibility to fully customize the sensor types and placement on the skin, it does not truly provide modularity as permanent silane bonds on the silicone do not allow for device disassembly.

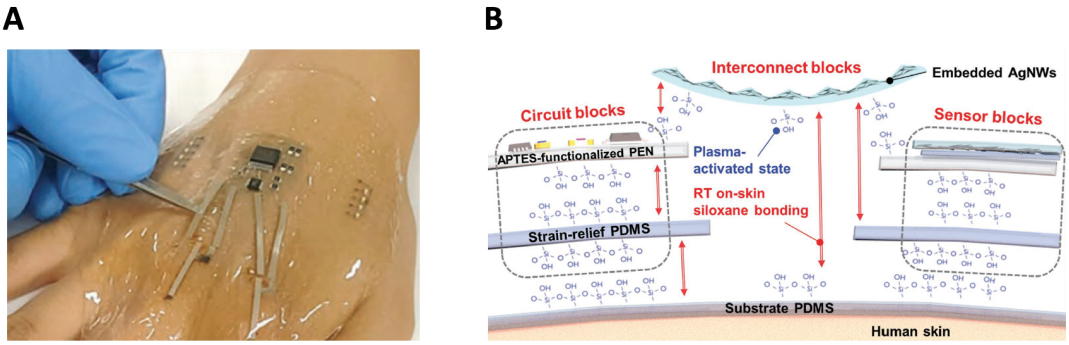

Figure 9: Stretchable modular sensor by bridging modules with a conductive composite strip. A) Placement of the interconnect conductive strips between functional electronics with the help of tweezers. B) Cross section schematic of the device process flow. Reproduced with permission of Yoon et al [48]

2.5 Thesis statement and contributions

This master's thesis aims to fabricate a modular stretchable system for on-body health monitoring applications. This technology would enable the creation of soft electronic modules that can be customized by the user and placed in any body location (wristband, chestband, headband) to provide multiple types of health related sensing (heart rate, motion, temperature). The device consists of two main components as shown in Figure 10: first, soft electronic modules with stretchable interconnections, and second, an electrical connector system that can join the soft modules together.

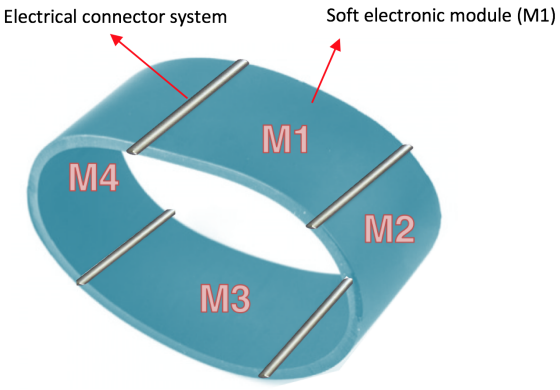

Figure 10: Example schematic of a modular and stretchable wearable band consisting of four soft modules (M1-M4) joined with an electrical connector system

Previous research on modular stretchable electronics has shown devices that either decrease performance when cut and rejoined [45] or are difficult to assemble given their ultra thin configurations [47, 48]. More specifically, these thin devices are designed to be worn as e-tattoos exclusively.

Unlike previous research, this modular stretchable system is designed to be worn as a wearable band (1mm thick) and its mechanism to assemble modules is user friendly and has high electromechanical performance.

To reach the thesis goal of making a modular stretchable wearable device, the work was split in two main objectives:

- **Integrating an electrically conductive stretchable material into a rubber substrate**. Techniques for making stretchable electronics are investigated and samples are fabricated onto soft rubber. Samples are electromechanically characterized using a uniaxial tensile testing machine. First, a tensile test until rupture is performed. If the material properties are satisfactory (over 50% strain with low changes in resistance) an additional sample is tested to fatigue by uniaxial tensile cycling (over 1,000 cycles).
- **Inventing a system to connect stretchable electronic modules**. A system for modular stretchable electronics is designed, fabricated and integrated with the previously developed stretchable conductive material. Samples are electromechanically characterized on a tensile testing machine and evaluated on-body by wearing the system as a bracelet and exercising on a treadmill.

3 An electrically conductive stretchable material on a rubber substrate

3.1 Introduction and evaluation metrics

This section represents the basis for making modular stretchable electronics. Without conductive stretchable lines embedded onto a soft substrate, it is not possible to integrate and evaluate the modular stretchable connectors that are made in the next chapter (Section 4). The material properties have to satisfy the following requirements:

- **Stretchability over 50% strain with minimum changes in resistance**. Human skin can stretch to a great extent. For example, movement on the fingers, wrist or elbows can cause deformations of about 40% 45% and 60% respectively [49]. Furthermore, limbs vary greatly in size depending on the subject. For example, the average adult wrist oscillates between 14 and 18cm in women and 16cm to 20cm in men [50]. Making a device that can deform from 14cm up to 20cm results in 43% stretch.
- **Easy to process and integrate with other components**. The conductive material should be well integrated with the rubber substrate. The chemical and physical properties of the elastomer are specially important when using conductive inks, as dissimilar materials tend to delaminate and cause electrical failures.

Two stretchable conductive strategies were developed and characterized: First, a commercial ink based on thermoplastic polyurethane (TPU) and silver deposited on polyurethane rubber (PUR), and second, a stretchable FPC using serpentine geometry manufactured by an external provider and encapsulated on extra soft silicone rubber.

Samples were prepared by depositing or embedding the stretchable material into a soft rubber film with four pads to perform a four-point resistance measurement. Samples were then electromechanically tested using a universal uniaxial tensile testing machine (Instron 5900), and resistance values were measured with an LCR meter (Agilent Keysight E4980a) and a dedicated Labview program that recorded the signal at 6.3Hz. If the uniaxial tensile test was successful (over 50% strain with minimal changes in resistance) the sample was tested to fatigue by applying a cycling strain over 1,000 cyles at 30% maximum deformation.

The four-point method for resistance measurements was used to electrically evaluate the samples, as it removed residual resistances added by the wires and contacts that connected the sample with the resistance meter. The main difference between this method and the common two-point method of probing is that the measuring device passes a current by two outer probes and measures the voltage by two inner probes (See schematic in supplementary Figure 38). The electrical properties of the material were obtained based on the sample resistance and its geometrical parameters. Equation 1 [51] represents the sheet resistance of a sample, where R represents the resistance, ρ the resistivity, W the width, T the thickness, L the length, R_s the sheet resistance

$$R_s = R \times \frac{W}{L} = \frac{\rho}{t} \tag{1}$$

3.2 Commercial TPU/Ag composites on PUR

3.2.1 Methods

As seen in the related work section 2.3, most of the commercial high conductivity inks are made of a mixture of TPU (Thermoplastic polyurethane) and silver. Inks are an interesting option for making stretchable electronics, as tracks can be printed fast and inexpensively onto a rubber substrate using stencils or direct printing. However, the elastomers should have similar chemical and physical properties as the inks that are printed on it, which is why manufacturers recommend printing TPU-based composites on TPU films.

Polyurethane (PU) elastomers are commonly synthesized by reacting a polyol molecule (an alcohol with two or more hydroxyl groups) and a diisocyanate [52]. There are multiple variations of PU depending on the polyol used, which can provide the rubber with different properties. For example, rubbers using a polyester polyol have good heat and oil resistance, while polyether polyols offer high resistance to moisture.

Amongst the polyurethane elastomers commonly found in the industry, one can find two types:

- **Thermoplastic polyurethane (TPU)**. Contains no cross-links between the polymeric chains and therefore can be dissolved with solvents to make conductive inks (e.g. silver-TPU) or heated up to 235°C to be processed using injection molding. TPU is available in pellets or sheets and must be dissolved or melted to process it. If TPU is mixed with a solvent, it is harder to control the viscosity and thickness of the screen-printed layer, as the solvent evaporates while processing it. Other options such as injection molding are too expensive in terms of equipment required.
- **Polyurethane rubber (PUR)**. Chains are cross-linked and the polymer is thermoset, which means the physical properties remain constant with temperature (no melting). A great advantage of PUR versus TPU is that it is commercially available as a two-part liquid rubber, which cures after mixing both components. Manufacturers claim negligible shrinkage after curing, and multiple hardnesses are available (Eg. from 30 Shore A up to 95 Shore A). The material is suitable for the device process flow, as films of PUR can be easily processed using screen printing techniques (with controlled thickness) and the multiple hardnesses are compatible with the soft-rigid interfaces necessary in this work (See Section 4.2).

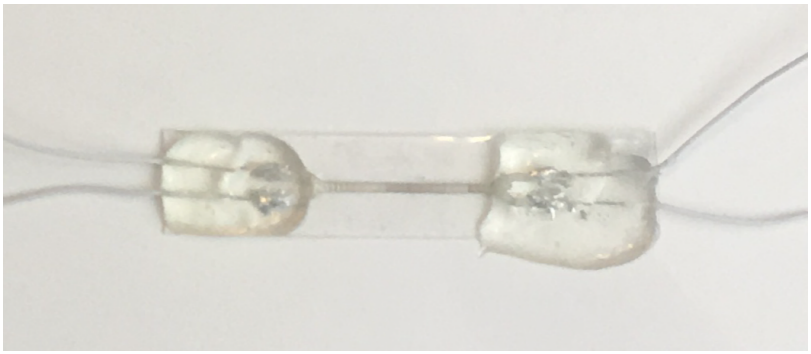

Figure 11: TPU/Ag ink sample screen printed in PUR with four wires for four-point resistance measurement

PUR of shore 30 hardness (Clear Flex 30, Smooth-On) was used as a substrate material and a conductive TPU-silver ink (PE874, DuPont) was chosen for the electrical stretchable lines. The processed PUR substrate had a thickness of 0.5mm and was deposited using a thin film applicator. The TPU/Ag ink was screen printed using a 125μm thick stencil and was oven cured at 130°C for 15 minutes.

Conductive samples were 20mm long and 0.75mm wide and have probes for measuring four-point resistance (See Figure 11). Samples were electrically interfaced with liquid gallium (EGaIn) and wires which were covered with a flexible encapsulation adhesive (3M, Scotch-Weld DP100 Epoxy Adhesive) and prepared following the process flow shown in Figure 12.

The PUR substrate was cured with three different protocols:

- **Room temperature and post curing**. Room temperature curing for 16 hours followed by a post curing at 60°C for 5 hours to remove the tacky surface as recommended by the manufacturer's technical bulletin.
- **Room temperature**. Room temperature curing overnight (12 hours) to preserve a tacky surface when screen-printing the silver ink.
- **Room temperature and solvent**. Room temperature curing for 12 hours and surface cleaned with acetone prior to screen-printing of the silver ink.

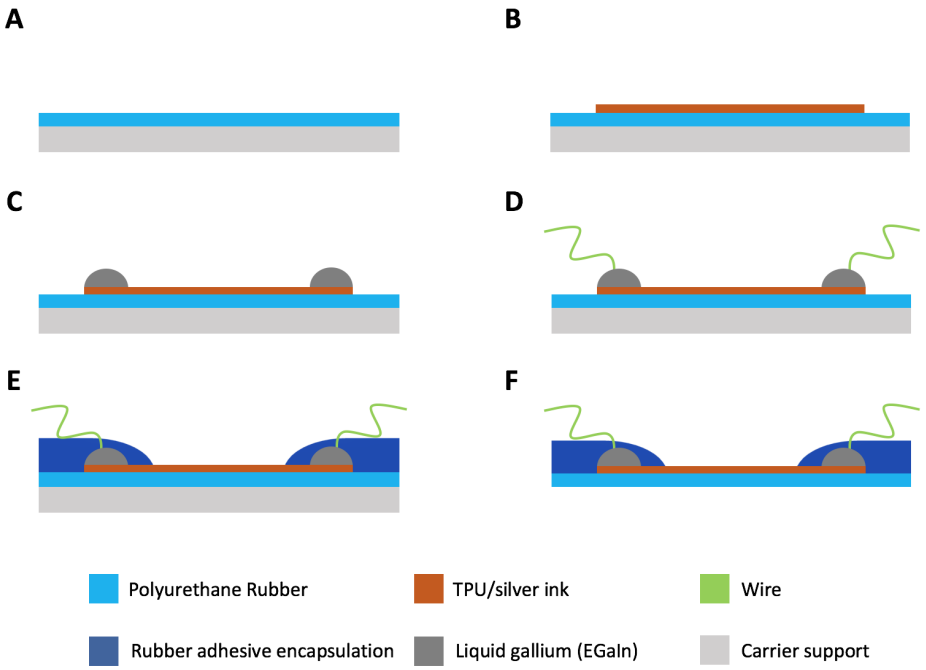

Figure 12: Process flow for preparing samples to characterize TPU/silver inks on PUR. A) Screen-printing of PUR on a glass carrier substrate and curing (room temperature or oven). B) Screen-printing of the TPU/silver ink on the rubber substrate. C) Placement of Liquid Gallium (EGaIn) on the connection pads. D) Adding wires to the EGaIn drops to interface the sample with the resistance measuring device. E) Addition of a rubber adhesive to encapsulate the connection pads. F) Removal of the sample from the carrier substrate

3.2.2 Results and discussion

As described in the methods section, three different polyurethane rubber preparation protocols were tested. Two samples were prepared for each protocol (6 samples in total). Samples showed high conductivity before testing with an average resistance of 0.245Ω (0.013 S.E.). Sheet resistance calculated with the geometrical sample parameters provided in the methods section 3.2.1 with equation 1 was $9.2{\cdot}10^{-2}\Omega$/sq, $5.2{\cdot}10^{-4}$ S.E. The electromechanical testing results and discussion for each of the three protocols used is described below:

- **Room temperature and post curing**. Results showed limited stretchability up to 3% strain maximum (See Figure 13A) for both samples after which the electrical connection was lost. One potential theory for such low performance is that PUR was completely cross-linked and the polymer chains were unreactive after depositing the silver ink. This theory led to the next experiment, which was curing the rubber to only 12 hours, so the rubber surface remained tacky. Potentially, the PUR would remain reactive, so the polymer chains from the TPU silver ink could make chemical bonds with the polymer.
- **Room temperature**. The changes in resistance vs strain reported in Figure 13B

showed similar results to the previous experiment. Samples could not be stretched over 3% strain without electrical failure. Even though the manufacturer (Smooth-On) did not disclose product formulations, some of their polyurethanes do not bond well to themselves, as they exude an oil that helps the demolding of certain materials [53]. It is theorized that such oil might be inhibiting the chemical reaction between the PUR and TPU. This leads to the next experiment, where the PUR surface is cleaned with solvent prior to depositing the ink.

- **Room temperature and solvent**. Results are almost identical to the previous two attempts, with stretchability ranges below 3% (Figure 13C).

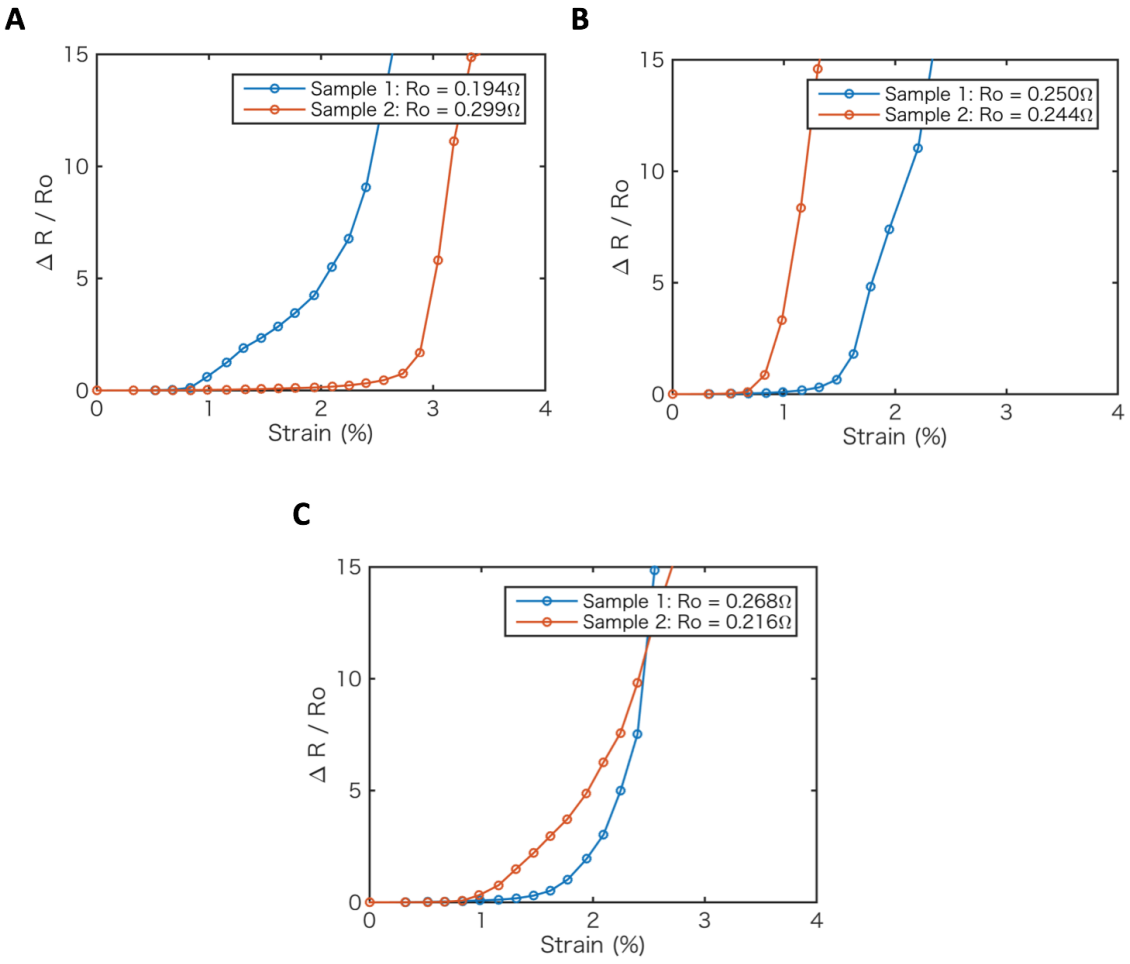

Figure 13: Electromechanical behavior of commercial TPU silver inks deposited on PUR with three different treatments. A) PUR cured at room temperature. B) PUR cured at room temperature and surface cleaned with solvent. C) PUR cured at room temperature and oven post cured.

Even though TPU and PUR should have very similar chemical formulations, it was not possible to make them react and bond to form a stretchable electric conductor that could

deform over 50% strain. PUR has proven to be chemically inert to TPU regardless of its curing protocol. Unknown factors such as different polyols used for each proprietary formulation could be the reason why the PUR rubber and TPU had poor bonding and delaminated.

Despite the low performance of the samples developed in this section, composites are still a promising solution as they can be easily processed using screen printing and can have extraordinary electromechanical properties. Some of the latest research in the field showed composites with resistivities as small as $1.62{\cdot}10^{-4}$ $\Omega{\cdot}cm$) that can stretch up to 400% [33]. This was achieved by using fluorine based elastomers, the inclusion of surfactants to help dispersion and specific curing protocols.

3.3 Stretchable FPC using serpentine geometries

3.3.1 Methods

There has been extensive research on how to optimize the shape of serpentine interconnects to have maximum stretchability. Figure 14 depicts the different geometric constraints that can be modified on a serpentine structure. Stretchability can be enhanced by lowering the w/R coefficient, while maximizing l/R and α [54–56]. On the other hand, high values of R and l would increase the overall trace width (Y), which is an undesired design parameter. Ideally, the connectors should occupy a limited physical space in the circuit (low Y values), meaning there is a trade off between size and stretchability. Given these constraints, the following parameters were chosen:

- Width (w): for the copper traces, 0.15mm was chosen given the fact that common flexible PCB manufacturers do not fabricate copper traces thinner than 0.1mm. Copper traces are then 'sandwiched' by polyimide slightly wider than the copper trace, as it increases device performance [27].
- Apha (α): Also equivalent to θ-90. A value of 30^o was chosen based on a simulation study [57] that found that stretchability of copper serpentines embedded on elastomer increases from 70% to 110% when α is increased from 0 to 30. However, further increasing α from 30 to 45 does not show a significant improvement in performance.
- Interserpentine legth (l): To avoid increasing the serpentine width (Y), the l value was disregarded ($l{=}0$).
- Radius (R) : Even though a higher radius implies higher stretchability, it also increments the serpentine amplitude (Y). A trade off value of 0.35mm radius was chosen to achieve maximum stretchability within the limited device width.

The maximum stretchability of coplanar serpentines is equal to the total length of the serpentine. This value can be also calculated if the geometric parameters of the coplanar interconnects are known by using equation 2, where ε_s represents the maximum stretchability of the serpentines and L, θ and R the parameters shown in Figure 14 [56].

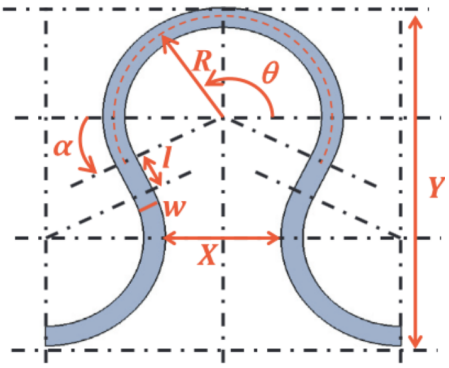

Figure 14: Geometric constraints of serpentine interconnects. The horseshoe design shown is a non-overlapping serpentine, X>0 with $\alpha = 30$ ($\theta = 120$). Reproduced with permission of Widlund et al. [54]

$$\varepsilon_s(\theta, \frac{L}{R}) = \frac{2\theta + \frac{L}{R}}{2sin\theta + \frac{L}{R}cos\theta} - 1 \tag{2}$$

For the configuration chosen of α=30 (θ=120), R=0.35mm and L=0mm, the maximum theoretical stretchability is 142%.

Given these parameters, testing samples containing two serpentines with top and bottom conductive layers were manufactured. The serpentine design was performed using AutoCAD software (Autodesk) and the final circuit design was made using Altium Designer software (Altium).

FPCs of 104μm total thickness were manufactured by Shenzhen JDB Technology Co. using a polyimide layer with double sided copper and a final polyimide coverlay to protect the copper layout. Further details about the FPC cross section can be found in Supplementary Figure 40.

Testing samples were prepared with the process flow shown in Figure 15. A layer of 0.5mm thick soft silicone (Ecoflex 00-30, Smooth-On) was screen-printed on a carrier substrate and oven cured at 65°C for 15 min, followed by the pick and placing of the stretchable FPC on the substrate layer.

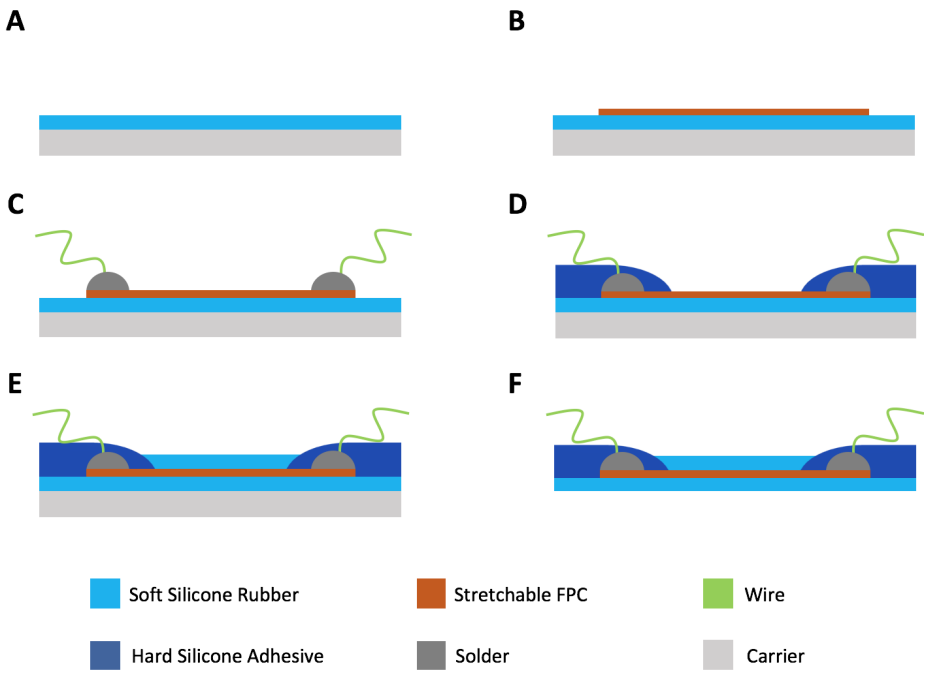

Figure 15: Process flow for preparing samples to characterize the stretchable conductors. A) Screen-printing of soft silicone on a carrier substrate and curing for 15 minutes at 65°C. B) Pick and placing of the Stretchable FPC on the elastomer substrate. C) Soldering of wires on the FPC connection pads. D) Pouring of a hard silicone adhesive to encapsulate the connection pads. E) Screen-printing of a final soft elastomer layer to encapsulate the FPC. F) Removal of the sample from the carrier substrate

To help the correct placement of the stretchable FPC on the substrate, a few drops of isopropanol (IPA) were added on the silicone surface. Sixteen wires were then soldered to the stretchable FPC for four-point resistance measurements (four wires for each of the four copper lines).

Next, hard silicone adhesive (Dowsil 734 flowable sealant, Dow Corning) was poured on the connection pads and was left curing overnight (12 hours). A layer of soft silicone was screen-printed with equal thickness and curing protocol as the first layer to encapsulate the stretchable FPC. Once the sample was removed from the carrier layer, it was ready for the electromechanical testing (Figure 16).

Samples were electromechanically tested using the same equipment as in section 3.2.1. Since four lines were tested simultaneously, resistance measurements were taken at 10% strain intervals instead of continuously.

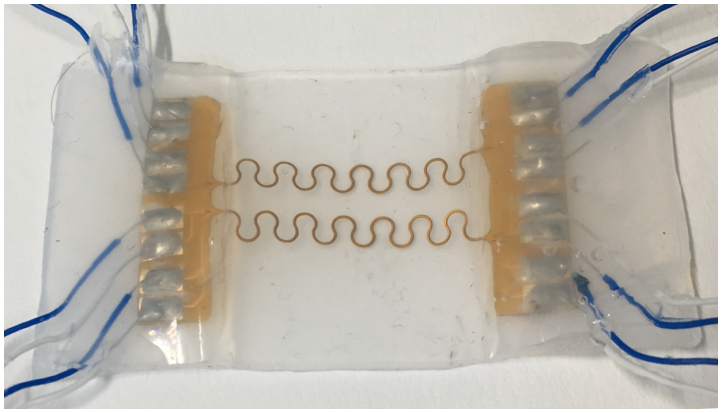

Figure 16: Stretchable FPC sample embedded in soft silicone with sixteen wires for four-point resistance measurement of its four conductive lines

3.3.2 Results and discussion

The electromechanical test for two independent samples (Figure 17) proved that the serpentines had practically no changes in resistance until 100% strain with an average of 0.45Ω. Past that range, the serpentines experienced a linear increase of their resistance up to 0.6Ω at 160%. Between 160% and 170% strain, both of the serpentines fractured and the electrical connection was lost.

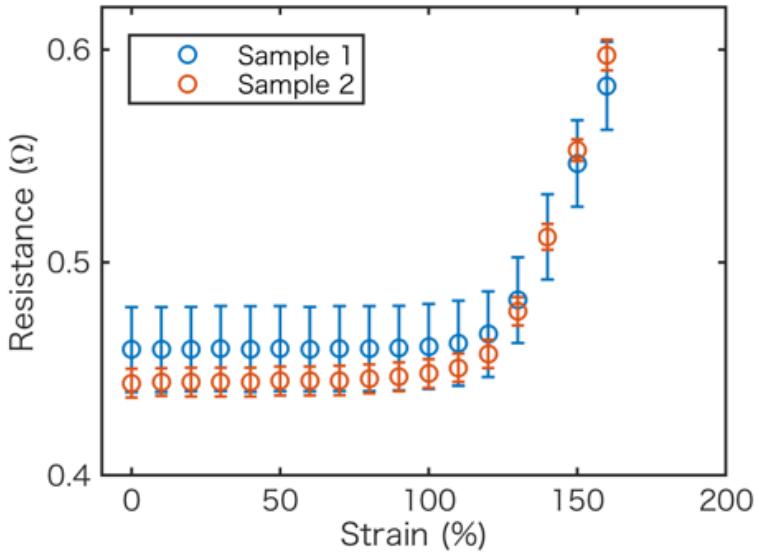

Figure 17: Resistance vs strain plot of two independent samples of serpentine FPC stretchable interconnections under uniaxial strain. Measurements were taken every 10% strain. Error bars correspond to the standard error of the four lines (two serpentines with both top and bottom conductive layers)

Electrical failure was confirmed with the crack of the serpentines as shown in the photographic sequence in Figure 18.

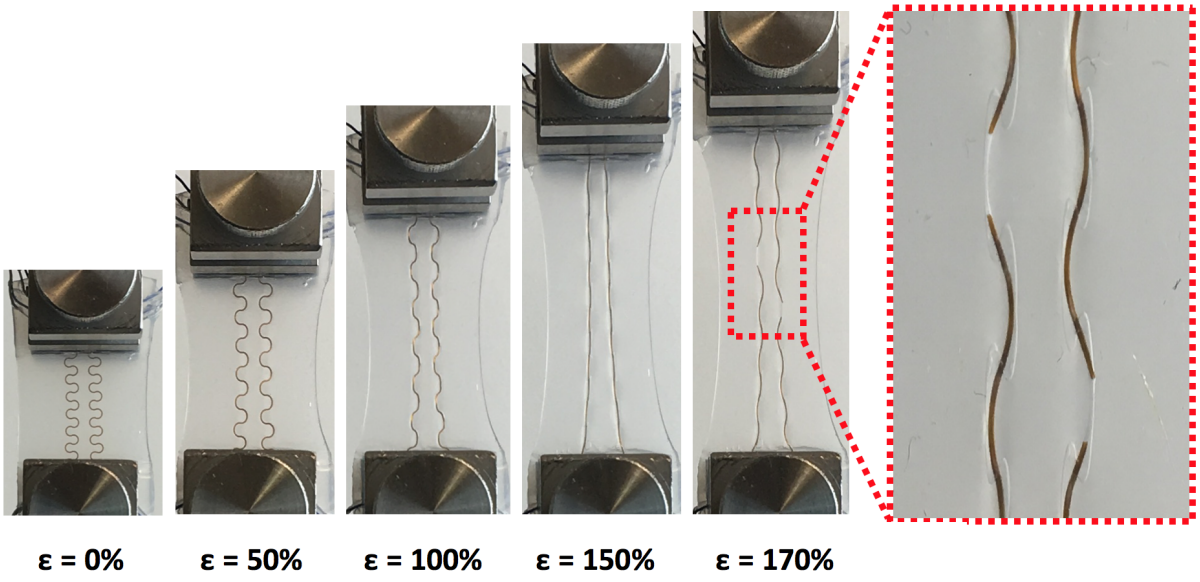

Figure 18: Photographic sequence of the serpentine FPC stretchable interconnections under uniaxial strain until electromechanical failure occurs

Error bars in Figure 17 represent the variability of the initial resistances for each of the four conductive lines. Supplementary Figure 39 shows the resistance changes for each conductive line (two serpentines, top and bottom layers). Samples experienced almost no variations in resistance (below 0.5%) until approximately 100% strain after which resistance values increased up to 25-30% before rupture at 160% strain. Each plot represents Serpentine 1 Top layer (Serp 1 Top), Serpentine 1 Bottom layer (Serp 1 Bot), Serpentine 2 Bottom layer (Serp 2 Bot) and Serpentine 2 Top layer (Serp 2 Top).

The average resistance of each line of the 25.5mm long serpentine was 0.443Ω. The maximum theoretical stretchability for serpentines with this geometry is 142%, as previously calculated in the methods section 3.3.1 using equation 2. However, the serpentine samples in this work showed stretchabilities over 160%. This can be explain by analyzing the stress-strain curve as plotted in Figure 19. Two distinct regions could be observed:

- **Buckling region**. Up to 90-100% strain, stress increased linearly at a 100% modulus of 93.9KPa (average between Sample 1 and 2). In this region serpentines changed from a 2D planar structure into a 3D shape by buckling. This mechanical deformation did not occur freely given the fact serpentines were embedded into an elastomeric substrate, adding stress to the sample while buckling. However, the rubber substrate was the main contributor of the sample's elastic modulus. Figure 19 depicts the stress-strain plot of the elastomer (Ecoflex, 00-30), assuming it deformed linearly up to the 100% modulus of 68.9KPa provided by the manufacturer's technical data sheet [58]. It can

be observed that at 100% strain, only 27% of the total sample stress (68.9 vs 93.9KPa) is caused by the serpentine structures.

- **Plastic region**. After 100% sample strain, the serpentine cross-section started to shrink as it continued transforming its 3D structure into a 1D line. Serpentines were made of a PI layer with double sided copper embedded into a PI adhered coverlay as seen in supplementary Figure 40. Copper can stretch up to 20%-40% elongation depending on material parameters such as processing temperature and phosphorous content [59]. On the other hand, polyimide can stretch up to 70% [60] (See supplementary Figure 41 for additional details), and it was assumed the proprietary adhesive is stretchable over 30% strain. These material properties may justify the extra deformation from the 142% theoretical maximum strain calculated in the methods section 3.3.1 up to the experimental 160-170% (18-28% difference). Another way to validate this plastic region was the approximately 30% increase in resistance seen in Figure 39 as the resistivity of a material varies proportionally with its cross section (see Equation 1).
  Once the serpentines rupture, the sample stress decreases from 330.9KPa at 160% strain down to 148KPa at 170% elongation, which is slightly over the estimated stress concentration of Ecoflex 00-30 at such strains (See yellow plot in Figure 19).

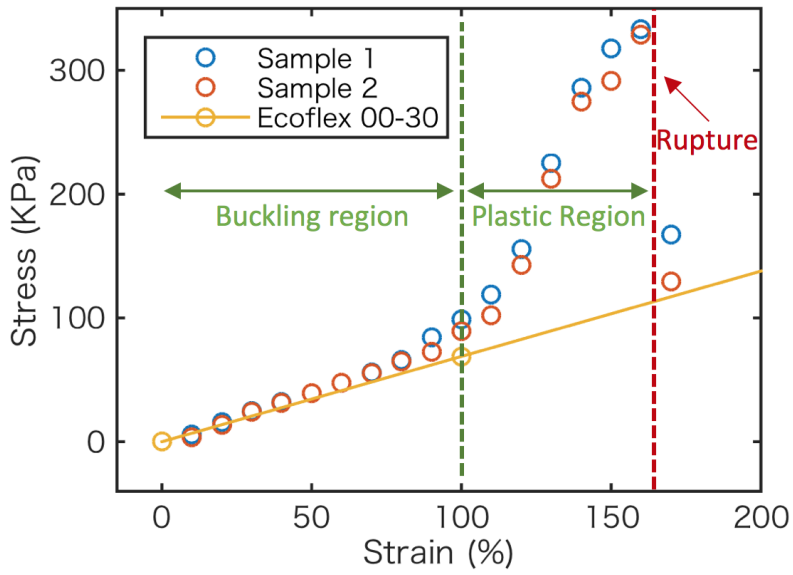

Figure 19: Stress vs strain uniaxial tensile test plot of the serpentine interconnects for two independent samples. The yellow line represents the stress strain plot of Ecoflex 00-30 (soft silicone used to embed the FPC) assuming the material deforms linearly up to 100% strain (100% modulus of 68.9 KPa) provided by the manufacturer's technical data sheet [58]. The dotted green line separates the buckling region from the plastic deformation region of the serpentines. There might be certain error with the values obtained as measurements were taken every 10% strain at different time intervals. Variations might be due to the viscoelastic behavior of the elastomer, geometrical relaxation of the serpentines within the elastomer and material creep in the plastic region

Given the high performance of the stretchable FPC samples, an additional FPC sample was tested to cycling strain up 10,000 cycles at 30% max strain. For this test, the four conductive lines were connected in parallel. The initial measured resistance was 0.118Ω, therefore each copper line had an average resistance of 0.472Ω (the inverse of the equivalent resistance of two or more resistors connected in parallel is equal to the sum of the inverses of the individual resistances). Results are shown in Figure 20.

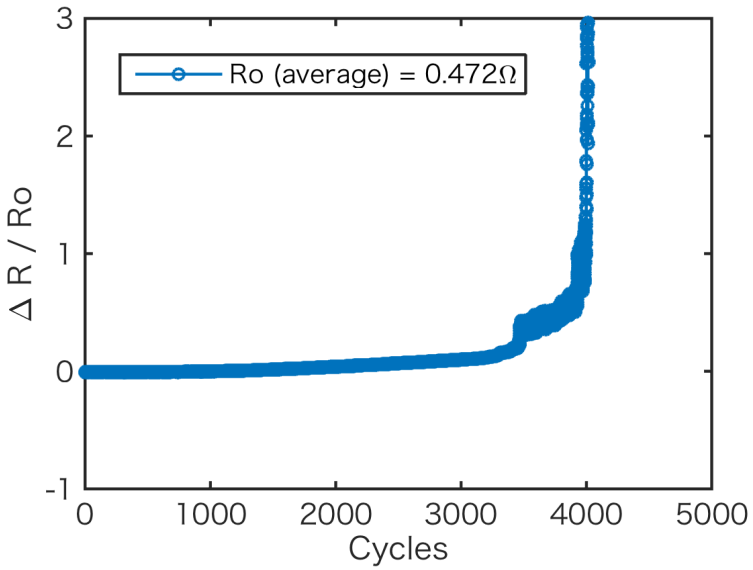

Figure 20: Electromechanical behavior of the stretchable FPC under a uniaxial tensile cycling at 30% maximum strain. Plot represents the relative changes in resistance as a function of applied strain and Ro the average resistance of each of the four conductive lines connected in parallel (measured Ro = 0.118Ω)

Results demonstrate the stretchable FPC has good resistance to fatigue up to 3,500 cyles at 30% strain. Over 4000 cycles resistance increases steeply due to fatigue damage of the copper wiring.

Since the serpentine performance is highly dependent not only on its geometric constraints but also on the substrate encapsulation (material and thickness) it is difficult to compare its performance to similar work in the literature. However, the high electromechanical performance under uniaxial strain obtained in this work (160 - 170%) is similar to other recent work in the literature reporting 171% [61].

High performance of the electromechanical cycling test at 30% maximum strain (up to 3,500 cycles) can be compared to similar commercial products. The company Fineline QPI develops stretchable PCBs based on copper and polyurethane encapsulation that can stretch up to 30% [62]. It can then be assumed that a 30% maximum stretch is desired for long term robust applications of this technology.

3.4 Conclusions

This chapter aimed to find a stretchable conductor that could be integrated into an elastomer and have satisfactory electromechanical properties (over 50% stretch with minimum changes in resistance). Two different techniques were attempted: the screen-printing of a commercial TPU based silver ink on PU rubber, and the encapsulation of flexible FPC designed serpentines into silicone. The following conclusions were drawn.

- Silver/TPU conductive inks screen-printed on PUR were highly conductive (average sheet resistance of $9.2{\cdot}10^{-2}\Omega$/sq, $5.2{\cdot}10^{-4}$ S.E.) but not electromechanically stretchable over 3% strain. Even though TPU and PUR materials were both based on polyurethane formulations, results showed poor bonding and delamination when stretched. Three treatments were made on the PUR prior to depositing the TPU/silver ink (fully cured, partially cured and surface cleaned with acetone), but they all achieved similar results.
- Flexible PCBs with serpentine designs embedded into soft silicone were highly electromechanically stretchable and conductive. Uniaxial tensile testing showed the material could stretch up to 100% with resistance values practically unchanged (0.44Ω for a 25.5mm long serpentine). This region corresponded to the geometrical buckling of the serpentines inside the elastomer.
- Past 100%, it is theorized the stretchable FPCs underwent a plastic deformation and its cross section shrinked. This was validated by the steep increase in mechanical stress (100KPa to 330KPa) and resistance (30% changes) of the copper traces.
- A fatigue test proved the stretchable FPCs could withstand 0-30% strain up to 3,500 cycles with minimum relative changes in resistance. After 4,000 cycles, the conductivity of the copper traces decayed steeply due to damage of the copper lines.

4 Four pin sliding connector for modular stretchable circuits

4.1 Introduction and evaluation metrics

When optimizing for device design and performance of the modular connector mechanism, the following key traits were pursued:

- **Low and ergonomic profile**. A successful modular stretchable device should be designed so it is almost not perceived by the user (little difference in size between a modular and non modular wearable band). However, soft thin films are difficult to manipulate, so the mechanism should have dimensions that are also user friendly (easy to open/close using fingers). Furthermore, it should contain a locking mechanism to prevent the device from falling once its worn on the body.
- **Ability to electrically connect four conductive lines**. One of the most popular serial bus communication protocols is the I2C (Inter-Integrated Circuit). I2C allows the communication of a master with multiple slaves by only using two lines (data and clock). When choosing this serial bus for device communication, the modular mechanism must connect four independent lines: power, ground, clock and data.
- **High electromechanical stability**. The mechanism should be able to withstand mechanical stresses when the device is stretched or worn with little changes in resistance across the conductive lines.
- **Easy to integrate with the device process flow**. The modular mechanism should be easily integrated as any other electrical component without additional steps in the process flow. This not only saves time, but makes it more feasible for mass manufacturing.
- **Easy to fabricate**. The fabrication process for making the stretchable mechanism should be fast, inexpensive and reproducible. Without this key trait, the modular device is not suitable for mass manufacture.

This chapter is divided into three parts. The first subsection covers the design and fabrication of the four pin sliding connector mechanism. Second, the connectors are electromechanically characterized using a uniaxial testing machine. Last, the electrical performance of the connectors is examined when samples are worn as a bracelet on a treadmill. Samples in the last two subsections are prepared by embedding the connector mechanism into stretchable serpentines as seen in section 3.3.

4.2 Connector design and fabrication

4.2.1 Methods

A novel mechanism to satisfy all the design and performance metrics was designed using 3D CAD software (Solidworks) (Figure 21). The design was optimized to have a low profile (ϕ4mm x 28mm) and be connected laterally in a similar user friendly and ergonomic fashion as the Apple Watch straps (as seen in Figure 4 in the introduction section 2.2). The

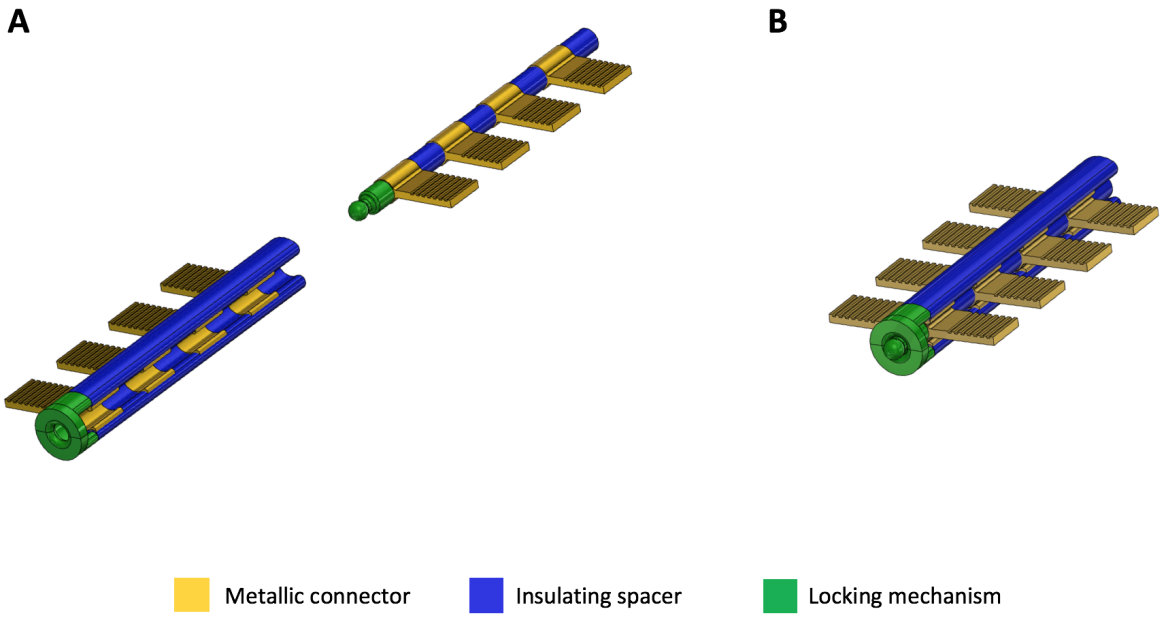

Figure 21: 3D model representation of the four pin sliding modular connector. A) Male (top) and female (bottom) modular connectors. B) Male and female parts electrically connected. The main three distinctive functional parts are colored: metallic connector (yellow), insulating spacer (blue) and the locking mechanism (green).

mechanism consisted of a male and a female part with four metallic connectors (represented in golden color) which could be attached by sliding one inside of the other (Figure 21B). The device also contained an insulating spacer (represented in blue color) to keep each of the four pairs of metallic pins electrically connected without shorting of the lines. Lastly, the device also had a locking mechanism (represented in green color) that added minimally to the device profile and prevented it from sliding out. This lock consisted of another male-female pair by inserting a sphere (on one side of the male part) into a tight tolerance hole (on the corresponding side of the female part). The sphere was designed to pop in and out easily with a gentle force applied by the user.

The modular mechanism design was also made to satisfy the requirement of easy integration with the target device process flow (See Figure 34). The connectors could be integrated with other electronic components within the same process flow step (Figure 34C). Each of the metallic pins contained a flat squared area to electromechanically connect the mechanism to the stretchable circuit using solder or conductive epoxy (Figure 34D). The area in contact with the stretchable circuit is then covered with hard rubber to make a soft-rigid transition to minimize stress concentrations (Figure 34E). The surface in contact with the hard rubber were designed with ridges to increase surface area and decrease stresses at the interface between the two materials.

The metallic connectors were made by cutting a brass sheet with high precision using

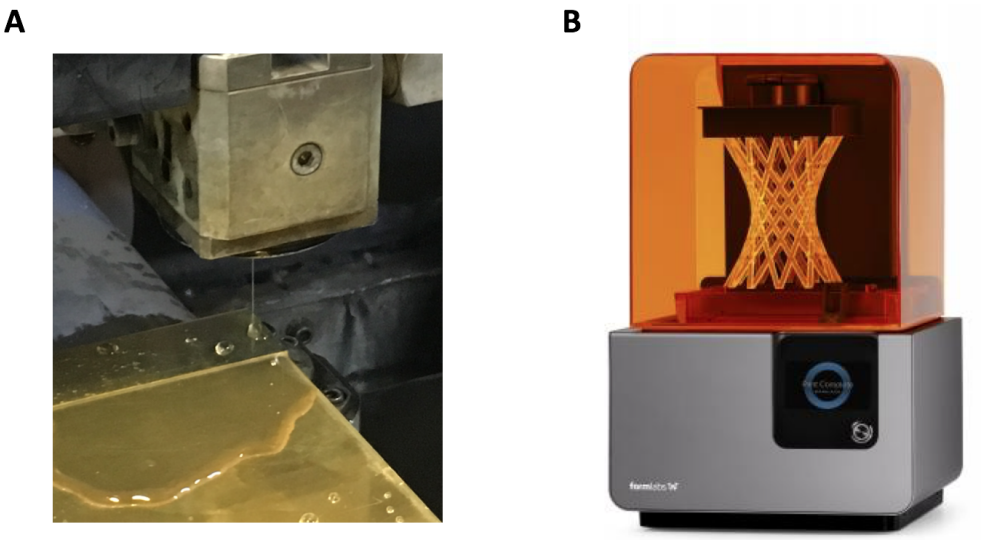

Figure 22: A) Electrical discharge machining (EDM) of brass to fabricate metallic connectors and B) Form 2 3D printer by Formlabs

an electrical discharge (EDM) machine (Sodick SL400G). This method of making brass connectors was compatible with mass manufacturing techniques, as it allowed cutting various metallic pieces simultaneously as well as stacking multiple brass sheets.

The insulating spacer and the locking mechanism were fabricated using a 0.025mm accuracy stereolithography printer with a clear resin (Form 2, Formlabs).

4.2.2 Results and discussion

A batch of 22 pairs of female and male connectors was fabricated by cutting a brass sheet on an EDM machine (as seen in Figure 23. Each piece could be easily snapped from its center piece by swinging each piece laterally 3-4 times with the fingers.

The 3D parts containing the insulating spacers and the locking mechanism were 3D printed and assembled with the brass connectors (Figure 24A). The final prototype looked very similar to the initial design in Figure 21 and a two-point resistance measurement test validated the electrical conductivity across the male and female parts.

Moreover, multiple pairs of female-male connectors could be manufactured and easily assembled in a repeatable manner, demonstrating its compatibility with mass production methods (Figure 24B).

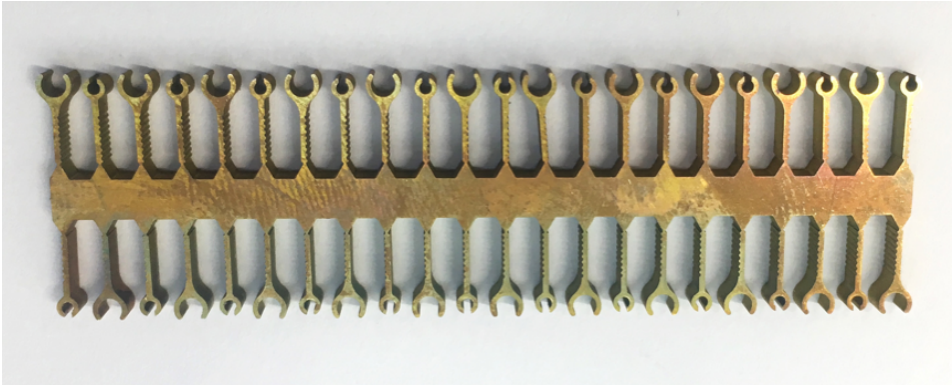

Figure 23: Fabricated batch of male and female brass connectors. Each piece could be easily removed from the core brass piece by snapping the thin section that connected them

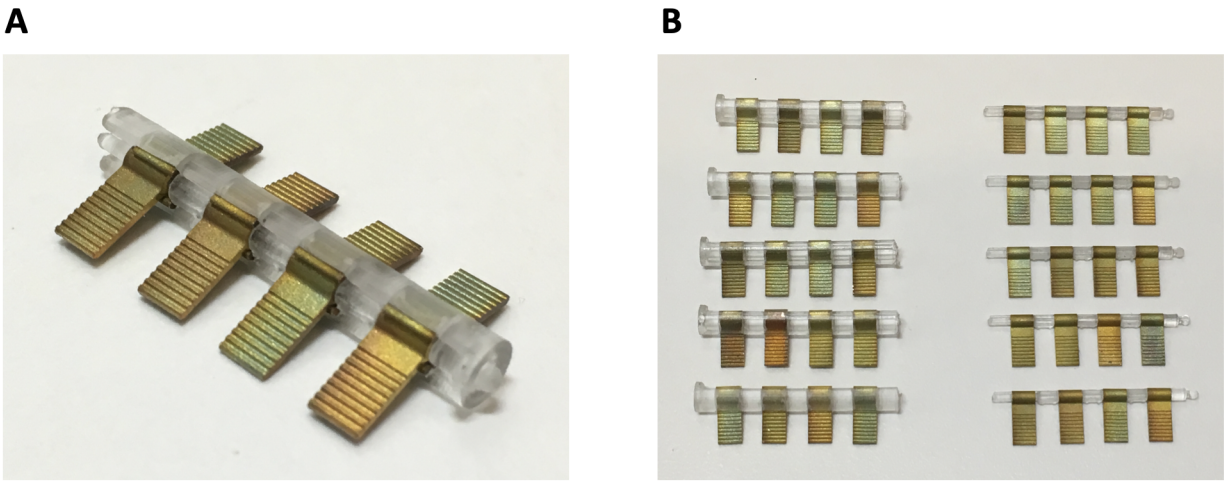

Figure 24: A) Final assembly of the four pin sliding connector mechanism (female-male pair connected) B) Batch of five assembled sliding connector female parts (left) and male parts (right)

4.3 Electromechanical characterization of the modular connector

4.3.1 Methods

The stretchable FPCs fabricated in section 3.3 were combined with the four pin connector mechanism to make a modular stretchable sample for electromechanical characterization. Samples consisted of two parts: one containing the male connector and another one with the female mechanism. On the sides of each sample part, eight wires were soldered for four-point resistance measurement to evaluate the resistance changes across the connector. Samples were prepared following the process flow in Figure 25.

The fabrication process had some common traits compared to the stretchable FPC samples (Figure 15). Same substrate material and thickness was used (0.5mm each side). However, the modular mechanism was connected to the FPC pads using a silver epoxy (8331 Silver Epoxy Adhesive, MG Chemicals). To do so, a thin 0.125mm layer of silver epoxy was screen-printed on the pads. Second, the modular connectors were placed on the epoxy and cured at 65°C for 15 min. Silver epoxy was used instead of solder paste because the 3D printed parts of the connector were made of a polymer resin that cannot withstand the elevated temperatures necessary to solder (usually over 200°C)

Figure 26 shows the final sample with both female and male parts connected, ready for testing. Each male and female part of the sample could be easily connected and disconnected by holding the sides with the fingers and sliding the device sideways (Figure 27) The same electromechanical testing protocol as seen in section 3.3.1 was used. The sample was stretched every 10% strain and values of four-point resistance and force for each connector were registered as well as the force value measured by the uniaxial testing machine. Sample stress was calculated by dividing the force values by the sample cross section (28mm x 1mm).

4.3.2 Results and discussion

Electromechanical failure of the modular stretchable samples occurred between 110 and 120% strain with the rupture of both serpentines. Values of equivalent serpentine strain (ε_s) shown in the photographic sequence in Figure 28 were obtained by dividing the stretch values by 0.721, which was equivalent to the proportion of the sample length containing the stretchable FPC. Failure between 110 and 120% translated into an (ε_s) between 153% and 166%. These results were consistent with the electromechanical test on the stretchable FPC samples in section 3.3.2 as serpentine samples failed between 160 and 170% strain.

Resistance values across the four conductive lines remained stable in a range between 1 and 2Ω. There was a small decay in resistance from 1.7Ω down to 1.1 Ω as the strain increased from 0% up to 80% respectively. This behavior was justified with the particular locking design of the modules. The device was designed to be placed on closed body regions (e.g. wrist, head, chest, etc) and tight to the skin. Therefore, the modules withstand a certain amount of tension, which kept the male and female parts secured, providing a stable electrical signal. Higher strain translated into higher contact forces between the male and female pins, slightly improving the conductivity.

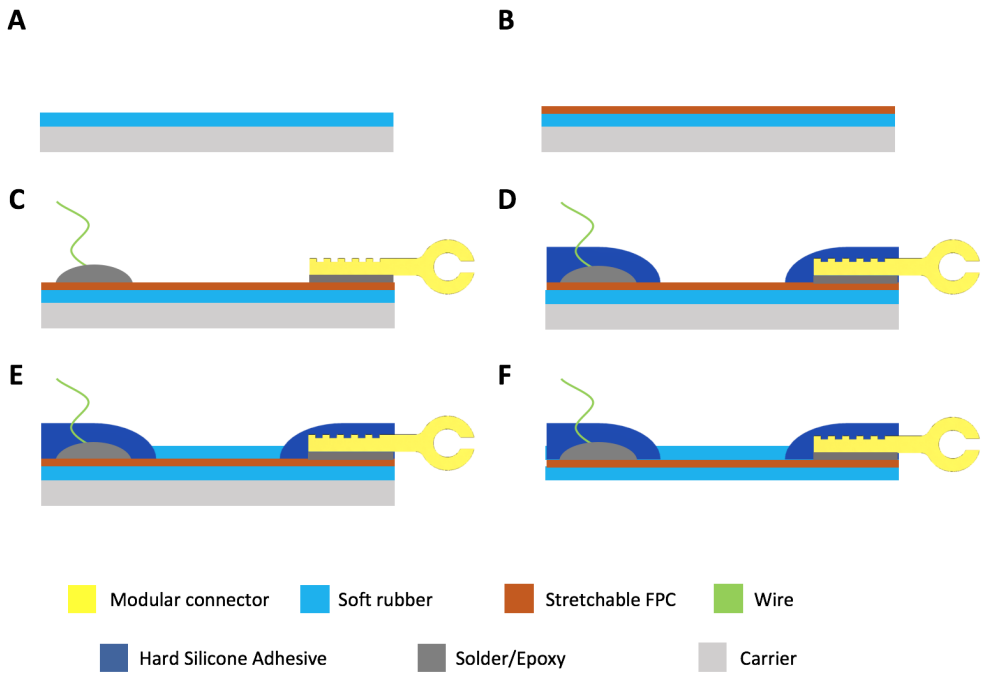

Figure 25: Process flow for preparing samples to characterize the modular connector mechanism. A) Screen-printing of soft silicone on a carrier substrate and curing for 15 minutes at 65°C. B) Pick and placing of the stretchable FPC on the elastomer substrate. C) Soldering of wires on the FPC connection pads and placing of the modular mechanism on previously screen-printed silver epoxy followed by oven-curing. D) Pouring of a hard silicone adhesive to encapsulate the connection pads and the modular mechanism E) Screen-printing of a final soft elastomer layer to encapsulate the FPC. F) Removal of the sample from the carrier substrate

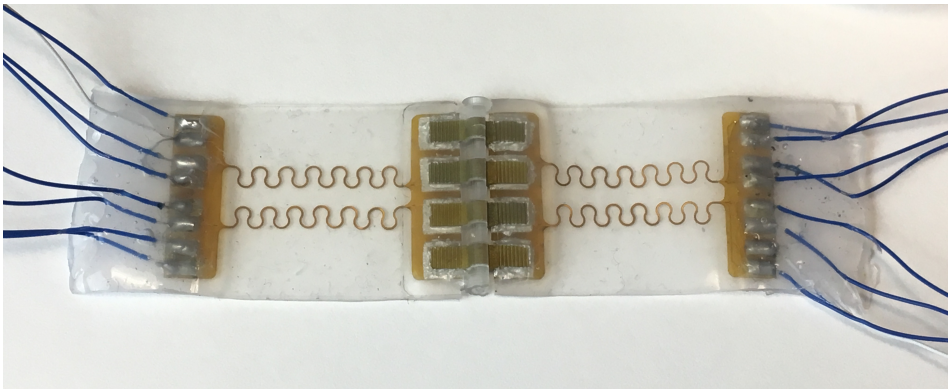

Figure 26: Modular connector sample connected to FPC stretchable serpentines ready for electromechanical testing

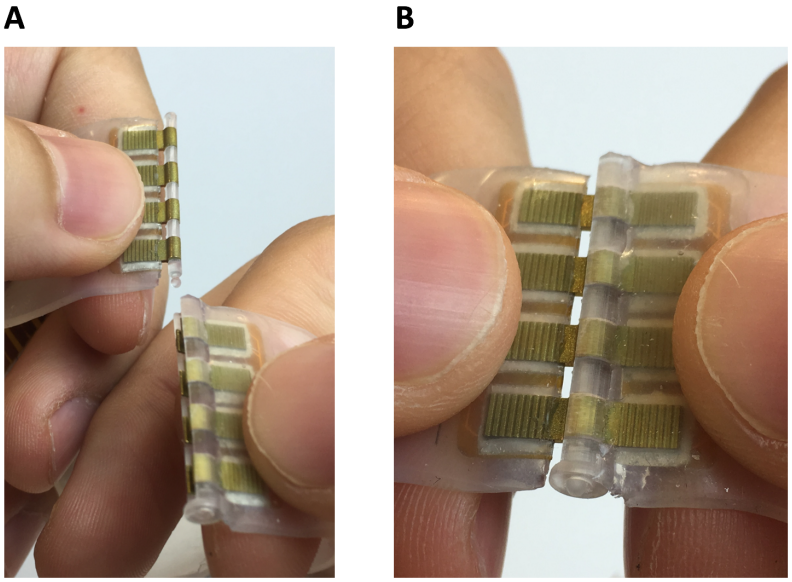

Figure 27: Connecting and disconnecting the modular connector sample. A) Disconnected. B) Connected

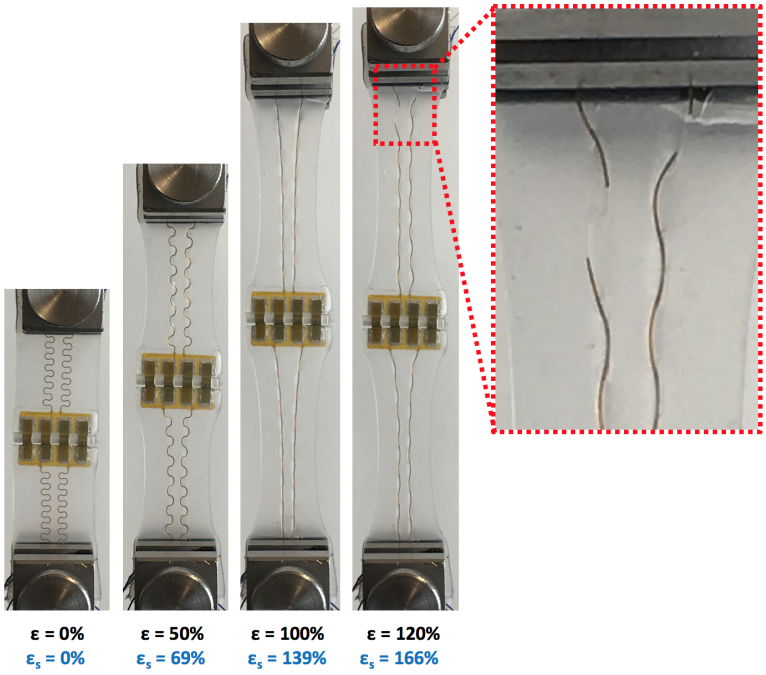

Figure 28: Photographic sequence of the stretchable modular system connecting two serpentine FPC stretchable interconnections under uniaxial strain until electromechanical failure occured. Values of ε_s corresponded to the equivalent strain sustained by the serpentines

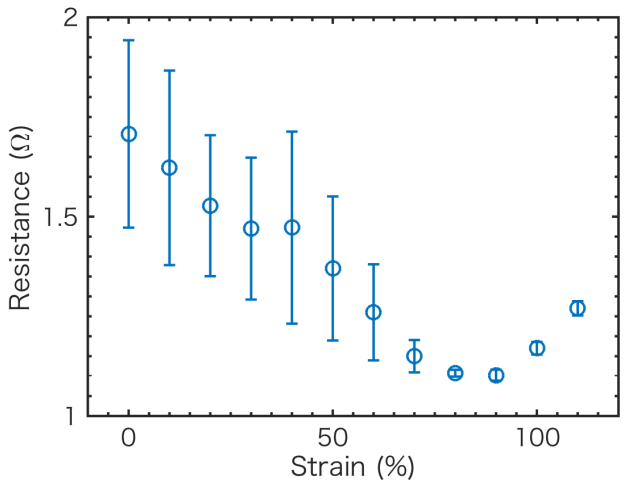

Figure 29: Resistance vs strain plot of the stretchable modular system connecting two serpentine FPC stretchable interconnections under uniaxial strain. Measurements were taken every 10% strain and error bars corresponded to the standard error of the four lines (two serpentines with both top and bottom conductive layers)

The results also show a decrease of the standard error of the mean from 0.24Ω down to 0.009 Ω within the 0-80% range. The variability across pins might be due to the difficulty to keep the metallic connectors perfectly aligned during the fabrication process (Figure 25C) which might cause that some connectors make better contact than others. However, increasing tension past 70% strain kept the value of each pin stable

From 80% strain until failure at 110%, resistance values increased 15% from 1.1 up to 1.27Ω. The 80-110% strain range converted into 111%-152% equivalent serpentine strain, which fell into the plastic deformation range of the stretchable FPC serpentines (See Figure 19). This justified the 15% change in resistance, as serpentines in the stretchable FPC sample increased resistances up to 30%.

Given the fact the serpentine average resistance was calculated in section 3.3.2, it was possible to estimate the average true resistance values at the module interface. The average resistance of each 25.5mm long conductive serpentine line was 0.443Ω. Since stretchable modules were made using two of the exact same serpentine modules, the total resistance of the stretchable section of the modular sample was approximately 0.89Ω. By subtracting the serpentine resistance from the values obtained in this experiment, it could be estimated that the true resistances at the module interface oscillated between 0.81 and 0.21Ω within the 0 to 80% strain range respectively. As a comparison, standard flex connector systems for flexible circuitry claim to have contact resistances as low as 0.02Ω [63] but still the connectors fabricated in this work satisfy basic requirements for digital communication.

On an I2C communication bus, high resistances could be an issue on the power line. Sen-

sors operate under a certain voltage range, and voltage drops on the power line could stop sensors from functioning. For example, a high accuracy temperature sensor (Si5051, Silicon Labs), operates at a current of 195nA and a voltage between 1.9 to 3.6V [64]. If a 3.3V standard supply is used, a voltage drop of 1.4V is needed to bring the electrical potential down to 1.9V. Using Ohms Law (V=I*R), a voltage of 1.4V at a current of 195nA requires a resistance of 7.2MΩ. This value is seven orders of magnitude higher than 0.81Ω, leaving a great safety margin.

However, other sensors bring this safety margin lower. An inertial motion unit (MPU6050, Invensense) has a minimum operating voltage of 2.375V working at a current of 3.6mA [64] and a PPG heart rate sensor (MAX86150, Maxim Integrated) has a voltage threshold of 3.1V at an operating current of 0.4mA [65]. Using Ohm's law, using a power supply of 3.3V contact resistances higher than 257Ω and 400Ω would cause failures to the IMU and PPG sensors respectively. Still, these values are three orders of magnitude higher than the 0.81Ω measured in this work, leaving a reasonable safety margin for connecting multiple modules together.

4.4 Electrical evaluation on a treadmill

4.4.1 Methods

The aim of this section was to further characterize the stretchable modular connector by wearing it as a bracelet and measuring changes in resistance while performing an experiment on a treadmill.

Bracelet samples were prepared by fabricating a modular stretchable sample (same process flow as in Figure 25) and joining both wire ends with RTV adhesive to make a loop and obtain a bracelet shape. Next, each of the 16 wires was soldered to thicker and four meter long cables to make the finished sample (Figure 30A). The device is then worn on the subject's wrist (16cm circumference) and it stays in tension at approximately 10% strain (Figure 30B).

During the treadmill test the cables of the bracelet sample were fixed in two distinct locations to prevent movement. One elastic band kept the cables close to the arm and a larger band held them to the chest. The remaining length of the cable was placed over the treadmill and exposed wires were connected to the LCR resistance meter (Agilent Keysight E4980a) with a Labview program that recorded four-point resistance values at 6.3Hz. The experimental setup is shown in Figure 31.

The treadmill experiment consists on measuring the resistance of each of the four pins in three cases. First, the subject stands still on the treadmill for 5 minutes (Figure 31A). Second, the user walks at a constant speed of 3 mile/h for 5 minutes (Figure 31B). Finally, the subject runs at a speed of 7 mile/h for 5 minutes (Figure 31C).

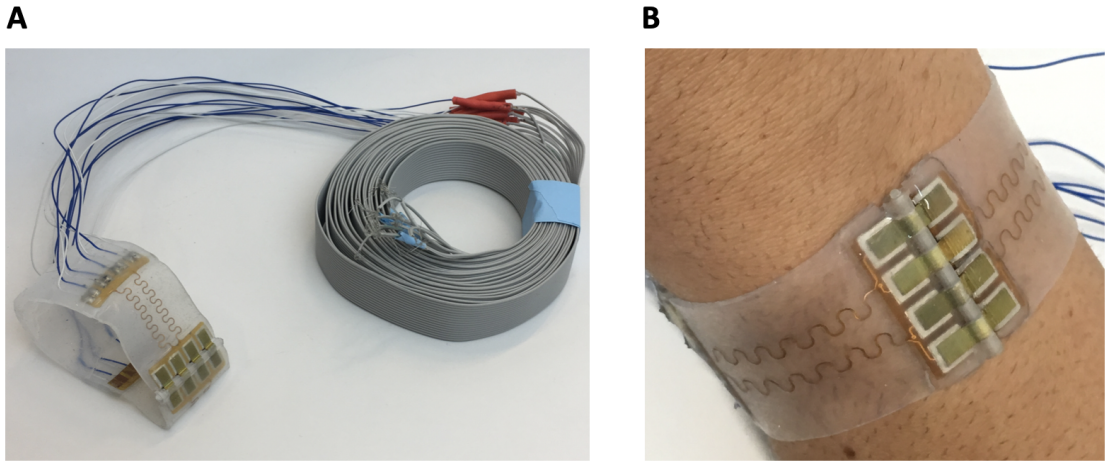

Figure 30: Bracelet sample to test the modular connector mechanism on a treadmill. A) Bracelet sample and the 16 wires that were connected to the LCR meter. B) Bracelet sample worn on the wrist

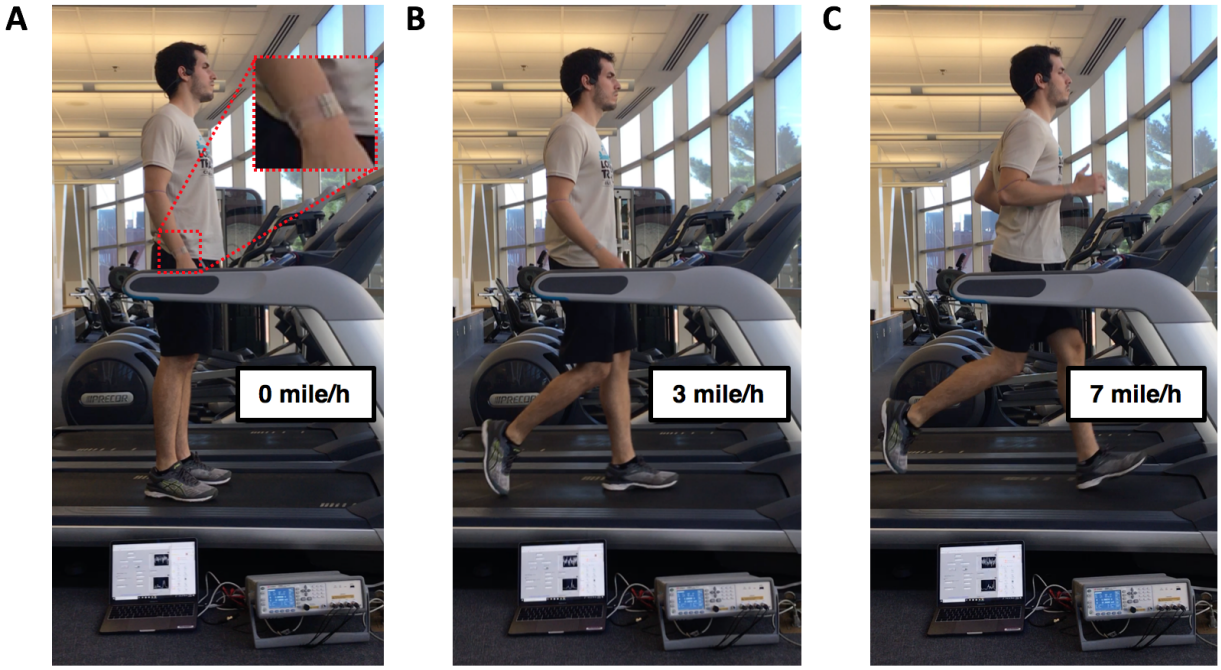

Figure 31: Electrical evaluation of the modular stretchable connectors on a treadmill under three different tests. A) 5 minutes standing still. B) 5 minute walk at 3 mph. C) 5 minute run at 7 mph. The bottom of the figure shows the LCR meter (right) and the Labview program that logs the real time data (left)

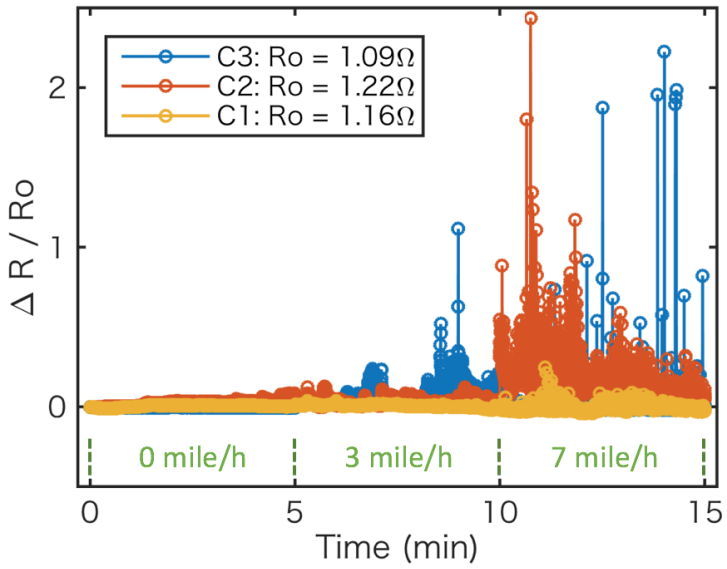

Figure 32: Relative changes in resistance during the evaluation of the modular stretchable connectors on a treadmill under three different tests. C1 C2 and C3 correspond to each connector pair measured. The fourth connector C4 could not be tested due to issues with the soldered cables

4.4.2 Results

The bracelet sample is made of four female-male brass connector pairs (C1 to C4) with wires to measure the electrical resistance across them. All connectors tested (C1, C2 and C3) had relative changes in resistance below 2.5 (Figure 32). The fourth connector (C4) could not be tested due to issues with the soldered cables.

Figure 32 also depicts different electrical behavior of the connectors depending on the activity performed. When standing still, changes in resistance were the most stable, below 20%. When walking, connectors experienced changes in resistance as high as 100%. When running, resistance fluctuated up to 250% (4.27Ω). Those changes were expected as running involved more aggressive arm movements than walking, exerting higher forces on the modular device.

The maximum changes in resistance for each connector were 0.24, 2.44 and 2.22 for C1, C2 and C3 respectively. As discussed in section 4.3 changes in resistance across different connectors were due to the difficulty to correctly align each of the four metallic parts during the fabrication process. Hence, some connector pairs might have had slightly more surface area in contact between them than others. Nonetheless, it could be concluded that all three connectors tested made stable electrical contact throughout each of the three parts of the experiment with low changes in resistance (4.27Ω max.).

These measured values were equivalent to the total resistance of two connected modules: both mechanism and serpentine lines (See Figure 26) . As previously calculated in section

3.3.2, two 25.5mm long conductive serpentine line modules have a total resistance of approximately 0.89Ω. By subtracting 0.89Ω from the measured values, the connector system resistance can be obtained. The 1.09 - 1.16Ω initial resistance when standing still (C1, C2 and C3 Ro, see Figure 32) is equivalent to 0.2 - 0.27Ω contact resistance and the maximum resistance of 4.27Ω when running is equivalent to 3.38Ω contact resistance. These values are slightly lower than the 0.81 - 0.21Ω measured in the experiment in section 4.3. This could be explained as wearing the device on the wrist keeps the male-female connector pair at an angle which might improve the contact surface. To lower this resistance value to the 0.02Ω of standard FPC connectors the contact surface could be enhanced with tin electroplating.

Device operation should not be an issue with resistances across the modules up to 4.27Ω. As previously discussed in section 4.3, resistances of 270Ω and 400Ω between the power and the sensor node would cause functioning failure a IMU and a PPG sensor respectively (electrical potential drops below the minimum operational voltage). This gives at least two orders of magnitude safety margin.

4.5 Conclusions

This chapter aimed to design, fabricate and characterize a connector for modular stretchable electronics. Device characterization was made by 1) electromechanically testing a connector pair embedded in stretchable FPCs as fabricated in section 3.3 and 2) Evaluating resistance changes when performing three different activities on a treadmill. The following conclusions were drawn.

- A four pin sliding connector was successfully designed and fabricated. The mechanism had a low profile (ϕ4mm x 28mm) and could be easily secured and removed with a lock mechanism placed on the side of the connector.
- The modular mechanism was easy to fabricate and was compatible with large scale manufacturing. The metallic parts were made of brass that was manufactured using an EDM machine. The insulating spacer and locking mechanism was made with 3D printed parts.
- The connectors could be easily integrated within stretchable FPC serpentines. It did not add steps on the process flow, making the assembly with stretchable conductors compatible with mass manufacturing techniques.
- The electromechanical evaluation of the modular connectors integrated into a stretchable FPC showed the device could be stretched up to 120% uniaxial strain until the rupture of the stretchable FPC matrix. Resistance values across each of the connector lines during the experiment were lower than 2Ω.
- The evaluation of the modular device worn as a bracelet on a treadmill showed electrical stability throughout the 15 minute experiment for each of the pins tested. Maximum peak resistance changes of 2.5 (4.27Ω) were found during the running experiment, while the base resistance when standing still oscillated between 1.09 and 1.16Ω.

- By subtracting the serpentine line resistance from the measured values in the treadmill experiment, the contact resistances of the modular connector when worn were calculated. The contact resistances when standing still oscillated between 0.2 and 0.27Ω, which are one order of magnitude higher than standard FPC connectors (0.02Ω). Contact resistance could be lowered if the conductivity at the male-female interface is improved (e.g. tin electroplating).
- Values of 4.27Ω across two stretchable interconnected modules should not interfere with the digital communication of sensors such as temperature, motion or heart rate. Only values of resistance larger than 270Ω on the power lines could cause voltage drops that interfere with proper device functioning.

5 Conclusions

This masters thesis focused on developing a system to connect stretchable electronic circuit modules. To do so, it was necessary to 1) Integrate an electrically conductive stretchable material into a rubber substrate and 2) Design and fabricate a system to connect stretchable electronic modules. The following conclusions have been drawn:

- Silver/TPU conductive inks screen-printed on PUR were highly conductive (average sheet resistance of $8.58{\cdot}10^{-2}\Omega$/sq, $4{\cdot}10^{-3}$ S.E.) but not electromechanically stretchable over 3% strain.
- Serpentine designed FPCs embedded into soft silicone had high electromechanical performance. The average resistance of a 25.5mm long conductive serpentine line was 0.44Ω. When embedded into 1mm thick silicone, serpentines could stretch up to 160-170% strain with minimum changes in resistance. When tested to fatigue, the stretchable FPCs could withstand 30% max tensile strain up to 3,500 cycles.
- A four pin sliding connector was designed and fabricated with low profile (ϕ4mm x 28mm), user friendly and compatible with mass manufacturing. The system was made using 3D printed polymer resin and brass parts cut with EDM. Also, it contained a locking system to prevent it from moving while worn.
- The connectors were well integrated with the stretchable FPC modules. Samples were made and electromechanically tested, showing the soft system could withstand strains up to 120% with values lower than 2Ω. The device proves to be robust as electromechanical failure occurs on the serpentine structure, not on the modular mechanism.
- The electrical evaluation of the modular device worn as a bracelet on a treadmill showed proper electrical stability. Maximum peak resistance changes of 2.5 (4.27Ω) were found during the running experiment. Such resistance values across modules should not interfere with the digital communication of sensors (HR, temperature, motion) as only values larger than 270Ω could cause voltage drops that interfere with device functioning.
- The contact resistances of the modular connector when worn oscillated between 0.2 and 0.27Ω when standing still. This value could potentially be closer to standard FPC connectors (0.02Ω) if the conductivity at the male-female interface is improved (e.g. tin electroplating).

6 Future work and preliminary results

Future work focuses on the multiple health-monitoring-related applications that could be built using the technology developed in this thesis. The main vision of this work is to give users the ability to customize their own soft electronics. For example, if a doctor wants to track the temperature and heart rate of a patient continuously, he can place a device with modules that sense temperature and heart rate on each temple. If a long distance runner is planning to track his\her heart rate and pace on a race, a chest-band could be assembled with a heart rate monitor, an accelerometer and multiple extra batteries. If a football player needs to track how his kicks are improving in terms of power, he can strap a device around his ankle to measure acceleration.

To reach this goal, a fabrication process flow that contained electronic components was developed. Five modules that could work with an I2C communication bus were designed and fabricated. I2C allows communication between sensor modules by daisy chaining them with clock and data wires and two pull up resistors (See Figure 33). The bus consists of a master module (dictating the speed of the clock), and the slaves (detecting and processing a start condition and recognizing its address)

The modules designed for this project consisted of a master, three slaves and an extra battery module as indicated below:

- Master module: contained the microcontroller (MCU) and a battery. Fanstel BC832 was chosen for the MCU given its small footprint and integrated bluetooth for wireless communication. The module also contained two pull-up resistors, an LED, a 12mAh battery with a switch and a 3.3V voltage regulator.
- Heart rate module: The MAX86150 PPG (photoplethysmography) sensor from Maxim Integrated was selected given its small footprint. A 1.8V regulator was needed for the internal LEDs of the sensor.
- Accelerometer module: The MPU6050 sensor from InvenSense was chosen, as only three resistors were needed for its operation.
- Temperature sensor module: The Si7051 chip from Silicon Labs was selected as it did not need any passive components for its operation and provided reliable values for biosensing (0.1°C accuracy)
- Extra battery module: contained a 12mAh battery with a switch and a voltage regulator.

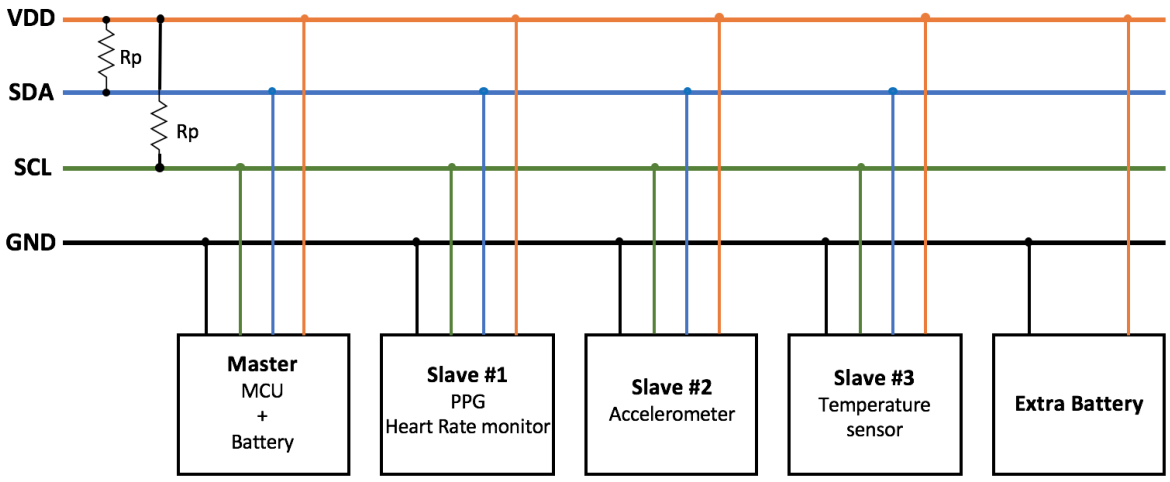

Figure 33: Electronic schematic of the five modules produced interconnected using an I2C communication bus. Two pull-up resistors (Rp) are needed for I2C communication. Modules consisted of a Master module with a battery and a micro-controller, three slaves (PPG, accelerometer and temperature sensor) and an extra battery

The stretchable FPC circuit was designed using Altium Designer and fabricated through an external vendor (Shenzhen JDB Technology Co., Ltd.) as in seen section 4.2. The soft modules were fabricated with the previously seen process flow in Figure 34 and with the same materials and protocols as in section 3.3.1. The main difference was electronic components and modular connectors were integrated in the same step (See Figure 34C and D).

Before following the process flow to fabricate the complete modules, the correct functioning of the electronics was checked by soldering the components to the FPC and connecting the pads to a breadboard with a MCU connected to a computer. Data was gathered from the MCU with the assistance of Dr. Artem Dementyev.

Five FPC stretchable circuits for each module can be seen in Figure 35 corresponding to the master, accelerometer, temperature sensor, PPG sensor and battery modules. The heart rate monitor was evaluated by connecting it to a MCU and reading data while placed on the wrist for a few seconds. Extracted data from the PPG device showed both IR LED and Red LED signal corresponding to three heartbeat peaks clearly defined (See Figure 36).

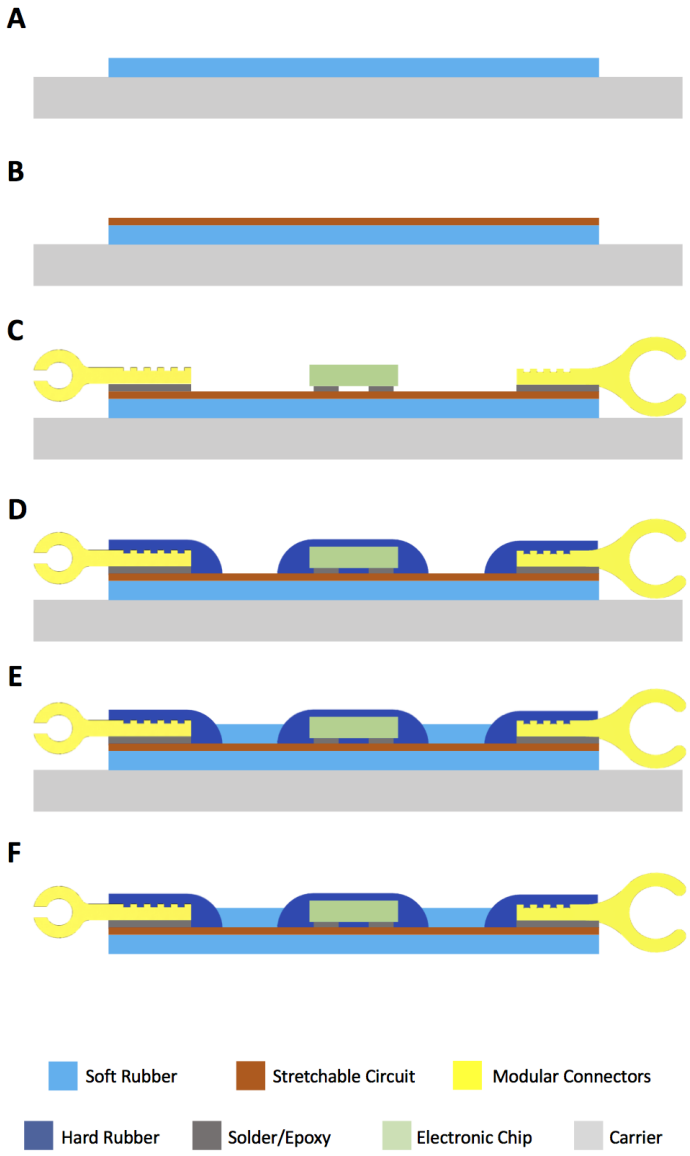

Figure 34: Process flow for making modular stretchable electronics. A) Screen printing of a soft rubber film on the carrier substrate. B) Placement or screen printing of the stretchable circuit. C) Screen printing of solder paste or conductive epoxy and pick and placing of electronic components and modular connectors. D) Encapsulation of the electronic components and modular connectors with hard rubber. E) Device encapsulation with soft rubber film screen printing. F) Device release from the carrier substrate.

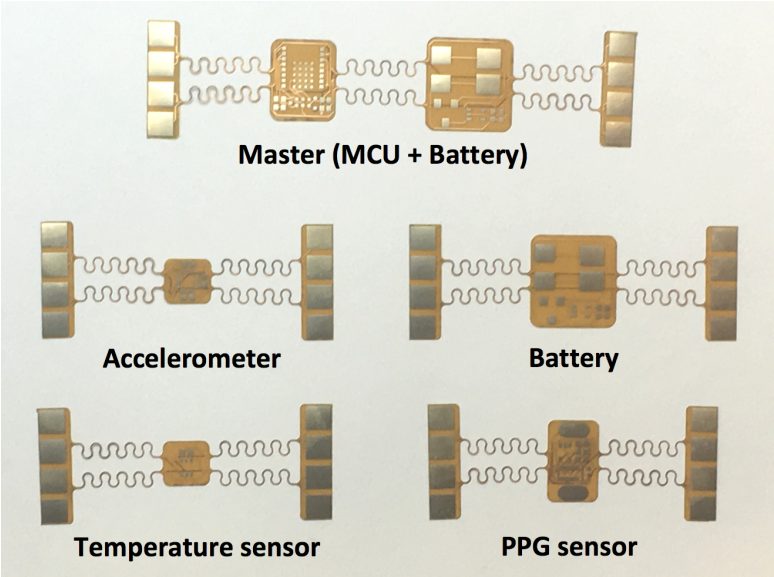

Figure 35: Five FPC stretchable circuits manufactured

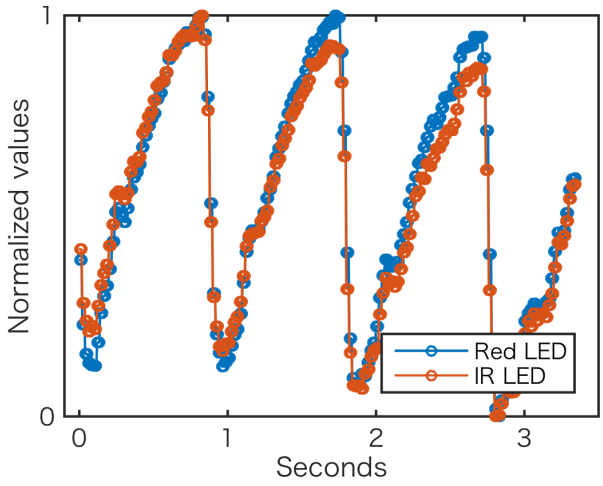

Figure 36: Signals measured from the heart rate module (Red LED and IR LED)

Next steps in this project involve:

- Checking the electronics for the rest of the modules (master module, accelerometer, temperature sensor and battery) by verifying they can successfully receive and transmit data.
- Integrating the stretchable FPC circuits into soft modules following the process flow in Figure 34.
- Exploring different module applications: wristband, headband, chestband or even 'ankleband'. Moreover, trying the possibility of using it as a sticker by adhering it to the skin with silicone adhesive. This could open other applications, for example tracking the movement of the knee with two accelerometer modules on top and bottom.
- Performing user studies to understand device comfort and usability compared to other off-the-shelf devices.
- Developing a mobile app to read data from the sensors wirelessly, continuously, and in real time.
- Placing two or more independent devices (more than one master) on different body regions to create a body sensor network. For example, one device placed on the leg could be used to track specific rehabilitation exercises while another one placed on the head measures heart rate and temperature.
- Further characterizing the device. The treadmill experiment in section 4.4 could be repeated by reading sensor data instead of resistance across metallic connectors. Also, the device could investigated for its adaptability to water proofness, given the fact the ability of the currently designed device to function underwater is unclear. Pins are in close proximity to each other and water resistivity could potentially short the lines.

Appendix

The following section contains supplementary figures that help better understand some of the concepts covered in this thesis (both theory and experimental data).

A Percolation threshold on composites made of conductive particles and elastomers

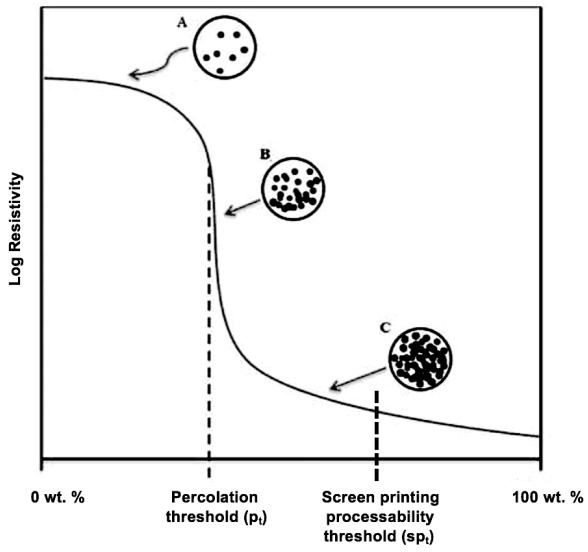

Figure 37: Electrical resistivity of a polymeric based composite vs amount of conductive filler. Percolation threshold (p_t) indicates the weight ratio (wt.%) at which the composite becomes conductive, whilst the screen printing processability threshold (sp_t) is the rate at which the viscosity of the composite is too high for using screen printing techniques

B Two-point vs Four-point resistance measurement

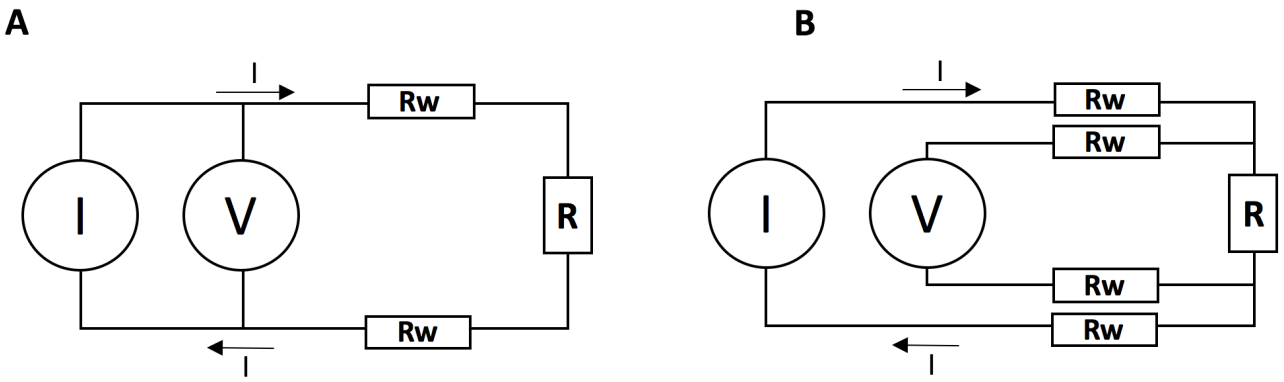

Figure 38: Two-point (A) vs four-point (B) resistance measurement. V represents a voltage meter, I a current generator, R the resistance to be measured and Rw the resistance of the wires and contacts

C Comparison of the four conductive lines of a two serpentine FPC under uniaxial strain

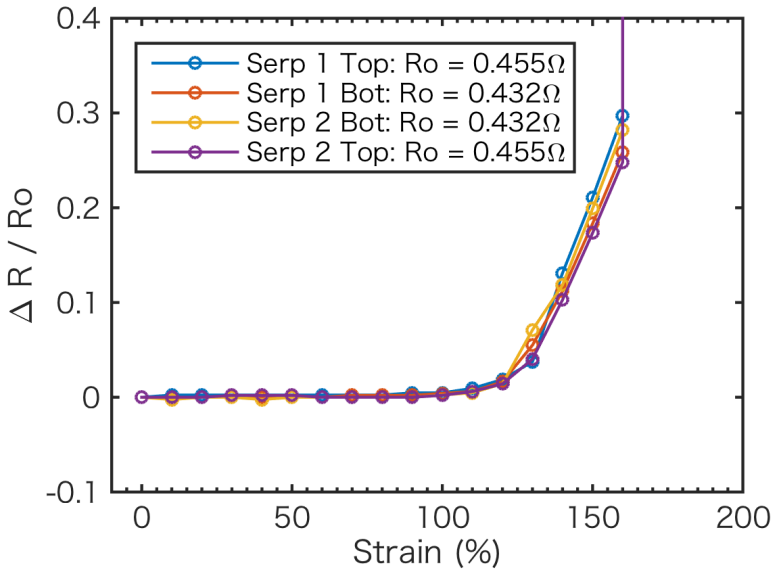

Figure 39: Comparison of the four conductive lines of a two serpentine FPC under uniaxial strain. Changes in resistance are practically inexistent (below 0.5%) until approximately 100% after which the serpentines increase up to 25-30% before rupture at 160% strain. Each plot represents Serpentine 1 Top layer (Serp 1 Top), Serpentine 1 Bottom layer (Serp 1 Bot), Serpentine 2 Bottom layer (Serp 2 Bot) and Serpentine 2 Top layer (Serp 2 Top)

D Cross section layers and dimensions of the FPC serpentines

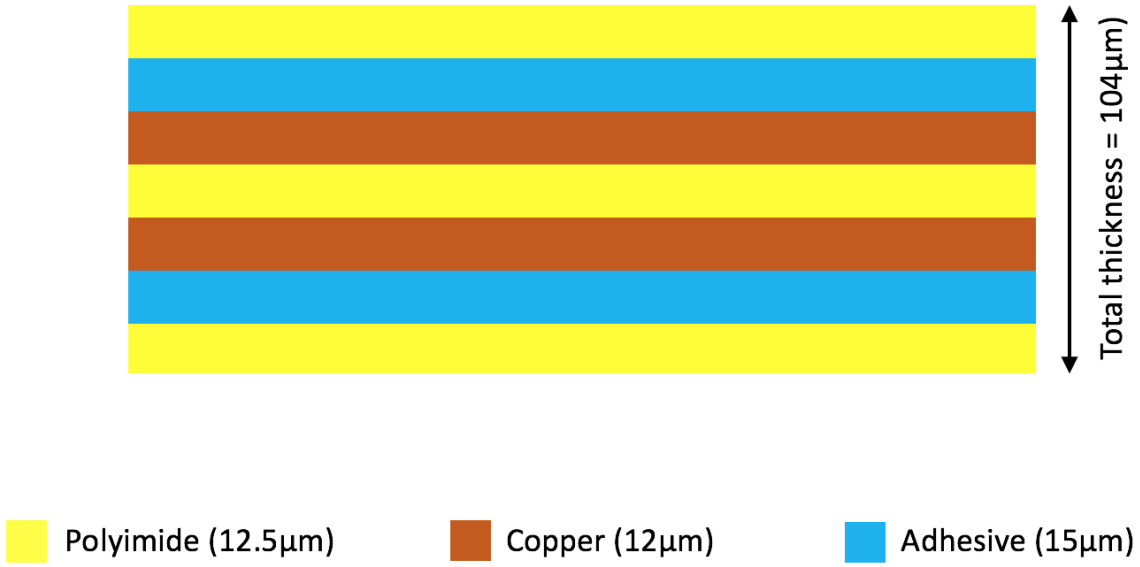

Figure 40: Cross section layers and dimensions of the FPC serpentines manufactured by Shenzhen JDB Technology Co., Ltd. Information was provided directly from the manufacturer

E Stress-strain curves of polyimide and copper

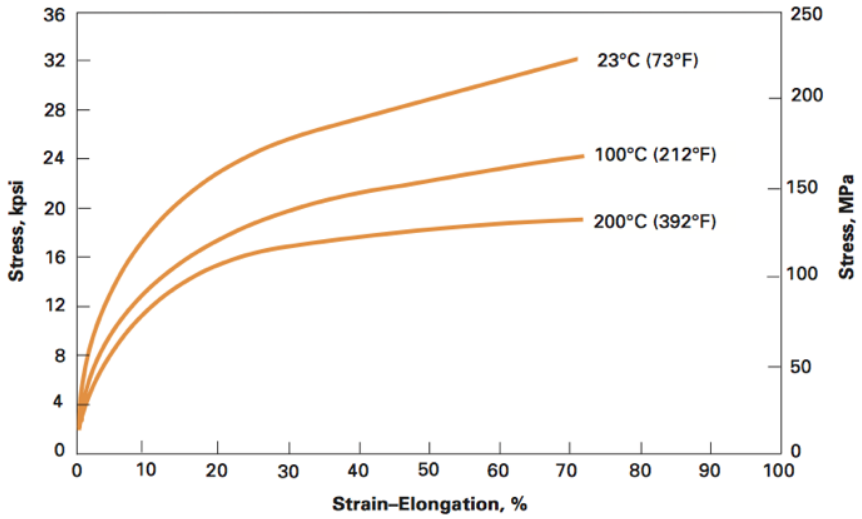

Polyimide (Kapton, Type HN Film)

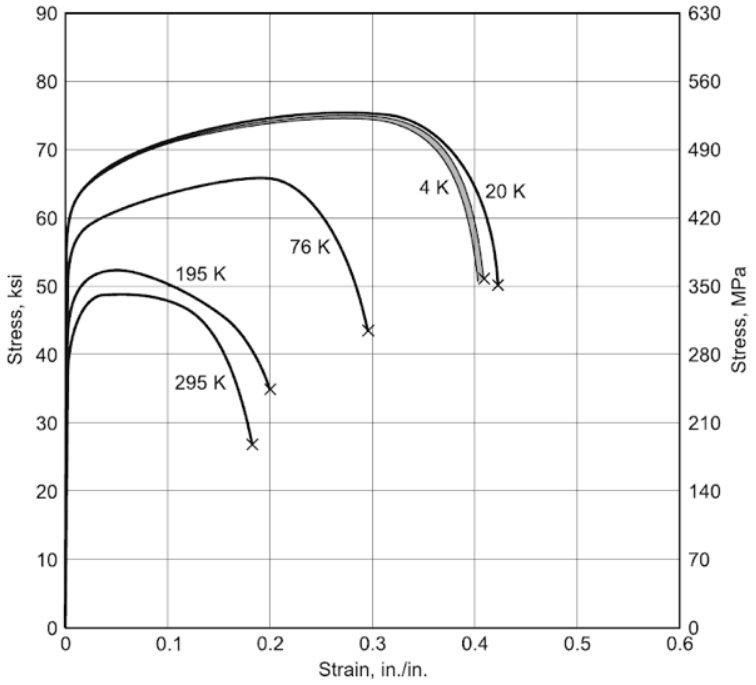

Copper (Oxygen-free, UNS C10200 bar)

Figure 41: Stress-strain curves of polyimide (Kapton, Type HN Film) [60] and copper (Oxygen-free, UNS C10200 bar) [59] processed at different temperatures

References

[1] D.-H. Kim, R. Ghaffari, N. Lu, and J. A. Rogers, "Flexible and stretchable electronics for biointegrated devices," *Annual Review of Biomedical Engineering*, vol. 14, pp. 113–28, 2012.

[2] D.-H. Kim, N. Lu, R. Ma, Y.-S. Kim, R.-H. Kim, S. Wang, J. Wu, S. M. Won, H. Tao, A. Islam, K. J. Yu, T.-i. Kim, R. Chowdhury, M. Ying, L. Xu, M. Li, H.-J. Chung, H. Keum, M. McCormick, P. Liu, Y.-W. Zhang, F. G. Omenetto, Y. Huang, T. Coleman, and J. A. Rogers, "Epidermal electronics," *Science*, vol. 333, no. 6044, pp. 838–843, 2011. [Online]. Available: http://science.sciencemag.org/content/333/6044/838

[3] P. Lamkin, "Smart wearables market to double by 2022: $27 billion industry forecast," *Forbes*, October 2018, accessed: 2018-10-26. [Online]. Available: https://www.forbes.com/sites/paullamkin/2018/10/23/smart-wearables-market-to-double-by-2022-27-billion-industry-forecast/#2ce044fa2656

[4] A. Marrington, D. Kerr, and J. Gammack, *Managing Security Issues and the Hidden Dangers of Wearable Technologies*, ser. Advances in Information Security, Privacy, and Ethics. IGI Global, 2016. [Online]. Available: https://books.google.com/books?id=yYXvDAAAQBAJ

[5] T. Carmody, "Is samsung's galaxy gear the first truly smart watch?" *MIT Technology Review*, September 2013, accessed: 2018-10-26. [Online]. Available: https://www.technologyreview.com/s/519051/is-samsungs-galaxy-gear-the-first-truly-smart-watch/

[6] "Garmin forerunner 935 tri bundle," https://www.triathletesports.com/garmin-forerunner-935-tri-bundle-2019/, 2018, accessed: 2018-10-26.

[7] L. Li, D. Paudecerf, and I. Yang, "Mechanical behaviour of natural cow leather in tension," *Acta Mechanica Solida Sinica*, vol. 22, p. 37–44, 2009.

[8] N. Herring and D. Paterson, *Levick's Introduction to Cardiovascular Physiology*. CRC Press, 2018, accessed: 2018-10-26. [Online]. Available: https://books.google.com/books?id=8yJWDwAAQBAJ

[9] K. Bonewit-West, *Clinical Procedures for Medical Assistants*. Elsevier Health Sciences, 2017, accessed: 2018-10-26. [Online]. Available: https://books.google.com/books?id=9Hc2DwAAQBAJ

[10] "Fitness trackers run into resistance over data security concerns," accessed: 2018-10-26. [Online]. Available: https://www.irishtimes.com/business/technology/fitness-trackers-run-into-resistance-over-data-security-concerns-1.3119483

[11] F. O'Connell, "Walking, jumping and resting, for the record," *The New York Times*, March 2013, accessed: 2018-10-26. [Online]. Available: https://archive.nytimes.com/www.nytimes.com/interactive/2013/03/14/technology/personaltech/Walking-Jumping-and-Resting-for-the-Record.html?_r=1&ref=technology

[12] "Nike+ fuelband 'ice'," *Nike News*, June 2012, accessed: 2018-10-26. [Online]. Available: https://news.nike.com/news/nike-fuelband-ice

[13] H. Somerville, "Jawbone's demise a case of 'death by overfunding' in silicon valley," *Reuters*, July 2017, accessed: 2018-10-26. [Online]. Available: https://www.reuters.com/article/us-jawbone-failure/jawbones-demise-a-case-of-death-by-overfunding-in-silicon-valley-idUSKBN19V0BS

[14] J. Phillips, "Jawbone explains up wristband failures and offers full refunds," *Wired*, December 2011, accessed: 2018-10-26. [Online]. Available: https://www.wired.com/2011/12/jawbone-explains-up-wrist-band-failures-and-offers-full-refunds/

[15] P. Miller, "Apple watch nike+ stomps on the ashes of the fuelband," *The Verge*, September 2016, accessed: 2018-10-26. [Online]. Available: https://www.theverge.com/2016/9/7/12761686/apple-watch-nike-plus

[16] A. Leather, "Blocks: The modular smartwatch that could crush all other wearables," *Forbes*, November 2015, accessed: 2018-10-26. [Online]. Available: https://www.forbes.com/sites/antonyleather/2015/11/18/blocks-the-modular-smartwatch-that-could-crush-all-other-wearables/#57c5ac7d6304

[17] A. Webster, "Nex band is a smart, modular charm bracelet for gaming on your wrist," *The Verge*, February 2014, accessed: 2018-10-26. [Online]. Available: https://www.theverge.com/2014/2/13/5289404/nex-band-is-a-smart-modular-charm-bracelet

[18] A. Dementyev, K. Hsin-Liu, and J. Paradiso, "Sensortape: Modular and programmable 3d-aware dense sensor network on a tape," *In Proc. of UIST*, vol. 82, 2015.

[19] C. Park and P. Chou, "Eco: ultra-wearable and expandable wireless sensor platform," *IEEE Body Sensor Network (BSN) Conference*, 05 2006.

[20] C. Vega, "Are you new to the apple watch? here's how to change an apple watch band," *Digital Trends*, 2017, accessed: 2019-4-26. [Online]. Available: https://www.digitaltrends.com/mobile/how-to-change-an-apple-watch-band/

[21] T. Tupper, "Ayah bdeir founded littlebits to make science fun. she might now be on to something bigger." *Forbes*, October 2015, accessed: 2018-10-26. [Online]. Available: https://www.forbes.com/sites/forbesinternational/2015/10/09/ayah-bdeir-founded-littlebits-to-make-science-fun-she-might-now-be-on-to-something-bigger/#3c9335b678b3

[22] M. Walton, "Roli blocks are expressive multitouch musical instruments for everyone," *Ars Technica*, November 2016, accessed: 2018-10-26. [Online]. Available: https://arstechnica.com/gadgets/2016/11/roli-blocks-mpe-midi-multitouch-musical-instruments/

[23] S. Lacour, "Skin health monitoring," *Nature Materials*, vol. 14, 2015.

[24] J. A. Rogers, T. Someya, and Y. Huang, "Materials and mechanics for stretchable electronics," *Science*, vol. 327, pp. 1603–1607, 2010.

[25] I. M. Graz, D. P. K. Cotton, and S. Lacour, "Extended cycling uniaxial loading of stretchable gold thin-films on elastomeric substrates," *Applied Physics Letters*, vol. 94, 2009.

[26] A. Chortos, J. Liu, and Z. Bao, "Pursuing prosthetic electronic skin," *Nature Materials*, vol. 15, no. 9, pp. 937–950, 2016. [Online]. Available: http://www.nature.com/doifinder/10.1038/nmat4671

[27] R. Verplancke, F. Bossuyt, D. Cuypers, and J. Vanfleteren, "Thin-film stretchable electronics technology based on meandering interconnections: fabrication and mechanical performance," *Journal of Micromechanics and Microengineering*, vol. 22, no. 1, p. 015002, 2012. [Online]. Available: http://stacks.iop.org/0960-1317/22/i=1/a=015002

[28] Y. Zhao and X. Huang, "Mechanisms and materials of flexible and stretchable skin sensors," *Micromachines*, vol. 8, no. 69, 2017.

[29] K. Harris, A. L. Elias, and H. Chung, "Flexible electronics under strain: a review of mechanical characterization and durability enhancement strategies," *J. Mater. Sci.*, vol. 51, pp. 2771–2805, 2015.

[30] S. Lacour and S. Wagner, "Stretchable gold conductors on elastomeric substrates," *Applied Physics Letters*, vol. 82, no. 15, p. p. 2404, 2003.

[31] S. Lacour, G. Courtine, and J. Guck, "Materials and technologies for soft implantable neuroprosthesis," *Nature Reviews Materials*, vol. 1, 2016.

[32] S. Rimdusit, C. Jubsilp, and S. Tiptipakorn, *Alloys and Composites of Polybenzoxazines*, 2013, no. July. [Online]. Available: http://link.springer.com/10.1007/978-981-4451-76-5

[33] N. Matsuhisa, D. Inoue, P. Zalar, H. Jin, Y. Matsuba, A. Itoh, T. Yokota, D. Hashizume, and T. Someya, "Printable elastic conductors by in situ formation of silver nanoparticles from silver flakes," *Nature Materials*, no. May, 2017.

[34] K.-y. Chun, Y. Oh, J. Rho, J.-h. Ahn, Y.-j. Kim, H. R. Choi, and S. Baik, "Highly conductive , printable and stretchable composite films of carbon nanotubes and silver," *Nature Nanotechnology*, vol. 5, no. December, pp. 853–857, 2010.

[35] O. A. Araromi, S. Rosset, and H. R. Shea, "Versatile fabrication of PDMS-carbon electrodes for silicone dielectric elastomer transducers," *IEEE Transducers Conference*, 2015.

[36] I. D. Joshipura, H. R. Ayers, C. Majidi, and M. D. Dickey, "Methods to pattern liquid metals," *Materials Chemistry C*, vol. 3, pp. 3834–3841, 2015.

[37] A. Hirsch, H. O. Michaud, A. P. Gerratt, S. de Mulatier, and S. P. Lacour, "Intrinsically stretchable biphasic (solid-liquid) thin metal films," *Advanced Materials*, 2016.

[38] D.-H. Kim, J. Xiao, J. Song, Y. Huang, and J. A. Rogers, "Stretchable, curvilinear electronics based on inorganic materials," *Advanced Materials*, vol. 22, no. 19, pp. 2108–2124. [Online]. Available: https://onlinelibrary.wiley.com/doi/abs/10.1002/adma.200902927

[39] S. Xu, Y. Zhang, et al., and J. A Rogers, "Soft microfluidic assemblies of sensors, circuits, and radios for the skin," *Science*, vol. 344, pp. 70–4, 04 2014.

[40] N. Matsuhisha, M. Kaltenbrunner, T. Yokota, H. Jinno, K. Kuribara, T. Sekitani, and T. Someya, "Printable elastic conductors with a high conductivity for electronic textile applications," *Nature Communications*, vol. 6, no. 7461, 2015.

[41] A. Maiti, W. Small, R. H. Gee, T. H. Weisgraber, S. C. Chinn, T. S. Wilson, and R. S. Maxwell, "Mullins effect in a filled elastomer under uniaxial tension," *Phys. Rev. E*, vol. 89, p. 012602, Jan 2014. [Online]. Available: https://link.aps.org/doi/10.1103/PhysRevE.89.012602

[42] S. Nagels, R. Ramakers, K. Luyten, and W. Deferme, "Silicone devices: A scalable diy approach for fabricating self-contained multi-layered soft circuits using microfluidics," *Langmuir : the ACS journal of surfaces and colloids*, vol. 29 20, pp. 6194–200, 2013.

[43] A. Tabatabai, A. L. Fassler, C. Usiak, and C. Majidi, "Liquid-phase gallium-indium alloy electronics with microcontact printing." *Langmuir : the ACS journal of surfaces and colloids*, vol. 29 20, pp. 6194–200, 2013.

[44] H. O. Michaud, J. Teixidor, and S. P. Lacour, "Soft flexion sensors integrating strechable metal conductors on a silicone substrate for smart glove applications," pp. 760–763, Jan 2015.

[45] J. Kang, D. Son, O. Vardoulis, J. Mun, N. Matsuhisa, Y. Kim, J. Kim, J. B.-H. Tok, and Z. Bao, "Modular and reconfigurable stretchable electronic systems," *Advanced Materials Technologies*, vol. 4, no. 3, p. 1800417, 2019. [Online]. Available: https://onlinelibrary.wiley.com/doi/abs/10.1002/admt.201800417

[46] J. Kang, J. B. H. Tok, and Z. Bao, "Self-healing soft electronics," *Nature Electronics*, vol. 2, no. 4, pp. 144–150, 2019. [Online]. Available: https://doi.org/10.1038/s41928-019-0235-0

[47] H. Jeong, L. Wang, T. Ha, R. Mitbander, X. Yang, Z. Dai, S. Qiao, L. Shen, N. Sun, and N. Lu, "Modular and reconfigurable wireless e-tattoos for personalized sensing," *Advanced Materials Technologies*, vol. 4, no. 8, p. 1900117, 2019. [Online]. Available: https://onlinelibrary.wiley.com/doi/abs/10.1002/admt.201900117

[48] J. Yoon, Y. Joo, E. Oh, B. Lee, D. Kim, S. Lee, T. Kim, J. Byun, and Y. Hong, "Soft modular electronic blocks (smebs): A strategy for tailored wearable health-monitoring systems," *Advanced Science*, vol. 6, no. 5, p. 1801682, 2019. [Online]. Available: https://onlinelibrary.wiley.com/doi/abs/10.1002/advs.201801682

[49] M. Amjadi, Y. J. Yoon, and I. Park, "Ultra-stretchable and skin-mountable strain sensors using carbon nanotubes–ecoflex nanocomposites," *Nanotechnology*, vol. 26, no. 37, p. 375501, aug 2015. [Online]. Available: https://doi.org/10.1088%2F0957-4484%2F26%2F37%2F375501

[50] J. H. Jewelry, "Measurement guide. measuring for bracelets, cuffs, and coils," accessed: 2019-8-2. [Online]. Available: https://www.johnhardy.com/bracelet-cuff-sizechart.html

[51] A. C. Diebold, *Handbook of Silicon Semiconductor Metrology*. CRC Press, 2001, no. 167.

[52] J. O. Akindoyo, M. D. H. Beg, S. Ghazali, M. R. Islam, N. Jeyaratnam, and A. R. Yuvaraj, "Polyurethane types, synthesis and applications – a review," *RSC Adv.*, vol. 6, pp. 114 453–114 482, 2016. [Online]. Available: http://dx.doi.org/10.1039/C6RA14525F

[53] Smooth-On, "Faq i attempted to add new rubber to an already cured urethane rubber mold and the new layer delaminated," accessed: 2019-8-2. [Online]. Available: https://www.smooth-on.com/support/faq/105/

[54] T. Widlund, S. Yang, Y.-Y. Hsu, and N. Lu, "Stretchability and compliance of freestanding serpentine-shaped ribbons," *International Journal of Solids and Structures*, vol. 51, no. 23, pp. 4026 – 4037, 2014. [Online]. Available: http://www.sciencedirect.com/science/article/pii/S0020768314003011

[55] S. Yang, S. Qiao, and N. Lu, "Elasticity solutions to nonbuckling serpentine ribbons," *Journal of Applied Mechanics*, vol. 84, 02 2017.

[56] H. Hocheng and C.-M. Chen, "Design, fabrication and failure analysis of stretchable electrical routings," *Sensors (Basel, Switzerland)*, vol. 14, pp. 11 855–11 877, 07 2014.

[57] M. Gonzalez, F. Axisa, M. V. Bulcke, D. Brosteaux, B. Vandevelde, and J. Vanfleteren, "Design of metal interconnects for stretchable electronic circuits," *Microelectronics Reliability*, vol. 48, no. 6, pp. 825 – 832, 2008, thermal, Mechanical and Multi-physics Simulation and Experiments in Micro-electronics and Micro-systems (EuroSimE 2007). [Online]. Available: http://www.sciencedirect.com/science/article/pii/S0026271408000760

[58] Smooth-On, "Technical bulletin ecoflex series," accessed: 2019-8-2. [Online]. Available: https://www.smooth-on.com/tb/files/ECOFLEX_SERIES_TB.pdf

[59] A. International, *Atlas of Stress-strain Curves*. ASM International, 2002. [Online]. Available: https://books.google.com/books?id=up5KS9fd_pkC

[60] DuPont, "Dupont kapton summary of properties," accessed: 2019-8-2. [Online]. Available: https://www.dupont.com/content/dam/dupont/products-and-services/membranes-and-films/polyimde-films/documents/DEC-Kapton-summary-of-properties.pdf

[61] E. Markvicka, G. Wang, Y.-C. Lee, G. Laput, C. Majidi, and L. Yao, "Electrodermis: Fully untethered, stretchable, and highly-customizable electronic bandages," pp. 632:1–632:10, 2019. [Online]. Available: http://doi.acm.org/10.1145/3290605.3300862

[62] F. Q. Group, "Stretchable pcb technology," accessed: 2019-8-2. [Online]. Available: http://www.qpigroup.com/en/products-services/pcb-technology/stretchable-pcb-technology

[63] Amphenol, "Flex connectors. clincher," accessed: 2019-8-5. [Online]. Available: https://cdn.amphenol-icc.com/media/wysiwyg/files/documentation/datasheet/flex/flexconnectors_254mm_clincher.pdf

[64] S. Labs, "Si7050/1/3/4/5-a20 i2c temperature sensors," accessed: 2019-8-5. [Online]. Available: https://www.silabs.com/documents/public/data-sheets/Si7050-1-3-4-5-A20.pdf

[65] M. Integrated, "Max86150 integrated photoplethysmogram and electrocardiogram bio-sensor module for mobile health," accessed: 2019-8-5. [Online]. Available: https://datasheets.maximintegrated.com/en/ds/MAX86150.pdf